Mathematical modeling of bacterial track-altering motors: Track cleaving through burnt-bridge ratchets

Blerta Shtylla and James P. Keener

Phys. Rev. E **91**, 042711 — Published 20 April 2015

DOI: 10.1103/PhysRevE.91.042711

Mathematical modeling of bacterial track-altering motors: track cleaving through burnt-bridge ratchets.

Blerta Shtylla
Department of Mathematics, Pomona College, Claremont, CA 91711

James P. Keener
Department of Mathematics, University of Utah, Salt Lake City, UT 84112

The generation of directed movement of cellular components frequently requires the rectification of Brownian motion. Molecular motor enzymes that use ATP to walk on filamentous tracks are typically involved in cell transport, however, a 'track-altering' motor can arise when an enzyme interacts with and alters its track. In *Caulobacter crescentus* and other bacteria, an active DNA partitioning (Par) apparatus is employed to segregate replicated chromosome regions to specific locations in dividing cells. The Par apparatus is composed of two proteins: ParA, an ATPase which can form polymeric structures on the nucleoid, and ParB, a protein that can bind and destabilize ParA structures. It has been proposed that the ParB mediated alteration of ParA structures could be responsible for generating the directed movement of DNA during bacterial division. How precisely these actions are coordinated and translated into directed movement is not clear. In this paper, we consider the *C. crescentus* segregation apparatus as an example of a track altering motor that operates using a so called 'burnt-bridge' mechanism. We develop and analyze mathematical models that examine how diffusion and ATP-hydrolysis mediated monomer removal (or cleaving) can be combined to generate directed movement. Using a mean first passage approach, we analytically calculate the effective ParA track cleaving velocities, effective diffusion coefficient, as well as other higher moments for the movement a ParB protein cluster that breaks monomers away at random locations on a single ParA track. Our model results indicate that cleaving velocities and effective diffusion constants are sensitive to ParB induced ATP hydrolysis rates. Our analytical results are in excellent agreement with stochastic simulation results.

I. INTRODUCTION

Many processes at the single cell level require the rectification of Brownian motion. Such a feat can be achieved in a multitude of ways and for a variety of cell processes. A so-called "biased-diffusion" principle often emerges as a force generating mechanism at the core of many cellular nano-machines [1, 2]. A fundamental and nontrivial question is how the bias is generated and maintained, and importantly, what are the relations that connect fundamental microscopic interaction rates with more mesoscopic scale quantities, such as drift velocity and effective diffusion constant.

Here we distinguish two main classes of biased diffusion force-generating mechanisms. In the first class, we have track-independent machines, such as ATP fueled molecular motors (i.e, dynein, kinesin etc) that use microtubule or actin filaments as tracks on which they 'walk' against a load by extracting energy from ATP hydrolysis [3]. This class of motors has received significant attention in the literature. In the second class, there are track-altering machines that can be broadly classified as particles that interact with and alter a substrate, or track; this reaction in turn changes or biases the particle motion. There are many processes that can be categorized as track altering motors, however, very few of them have received attention in the modeling literature. A well-studied example of this second class of motors occurs for collagenase transport along collagen fibrils, where directed movement is achieved as a result of proteolysis, or cutting of fibrils, by collagenase [4, 5]. Theoretical models that address various aspects of collagenase cleaving have been proposed in the literature [6–8]. This class of track-altering motors can be naturally extended to include the propagation of hydrolysis/autocatalytic reaction waves [9, 10], as well as the dynamics of molecular DNA biped constructs [11, 12]. Most of the mathematical models on track altering motors fall into the category of so called 'burnt-bridge' mathematical models.

Burnt-bridge models are simplified theoretical constructs used to understand the dynamic properties of track-altering molecular motors [5–9, 13, 14]. In the standard burnt-bridge model (BBM), a protein complex is viewed as an unbiased random walker that hops around a one-dimensional discrete polymer lattice. The lattice is composed of strong and weak links. The random walker does not affect the strong links, but the weak links can be destroyed with probability $0 < p \leq 1$ when the walker passes them. The key assumption in BBM is that once a bridge is burnt, the walker cannot cross it again; this allows for the walker to remain associated with the track. Depending on the rules imposed for bridge-burning, BBM models are classified into two categories: 1) forward BBM, where bridges can be burnt if passed by the walker in one direction only, 2) forward-backward BBM where the bridge is burnt if passed from either direction. The forward and the forward-backward BBM models are indistinguishable if the probability of bridge destruction is $p = 1$, however random walker dynamics show some difference for these two models for the more general case where the bridge breaking probability is less than one. In the one dimensional lattice case, where the protein walks on a single track, systematic theoretical studies have been proposed, however, these studies are often limited in scope. Limiting cases have been studied for a continuous-time, continuous-space model with $p << 1$ and $p = 1$ [5, 9]. Discrete-time approaches have also been applied to calculate mean drift velocities and dispersion coefficients (dispersion was only given for $p = 1$) [15]. Continuous time models have been used to study one dimensional burnt-bridge lattice [7, 13].

In this study, we describe a biological process where models of track-altering motors can be useful. Specifically, we are concerned with a class of path-modifying molecular motor constructs that appear in bacterial cell division. DNA segregation in some classes of bacterial cells is a well controlled process involving a set of ATPase proteins that dynamically interact with a chromosome and facilitate its movement to specific locations in the cell [16, 17]. In these cells, Plasmid associated proteins (Par) form dynamic assemblies that guide the segregation of a replicated chromosome copy to specific locations in the cell. In the case of *Caulobacter crescentus* bacterium, ParA proteins are slow ATPases that can form linear polymeric assemblies that dynamically assemble and disassemble inside of the cell, reminiscent of cytoskeleton dynamics of eukaryotic mitotic cells [16]. Similar Par cytoskeletal-like systems work in *E. coli* bacterium to dynamically reposition plasmids inside cells [18, 19]. In *Crescentus*, ParA filament assembly first requires a dimerization reaction between two ParA monomers and two ATP molecules, and subsequently the resulting dimers can be combined into filaments [16], or continuous nucleoid-associated patches [20]. On the other hand, ParB proteins associate and cluster on a specific chromosomal site and also have binding affinity for ParA dimers. ParB proteins can hydrolyze ATP and in doing so they cause the breaking of the ParA track that they associate with (we refer to this action as track-cleaving). Directed chromosome segregation in these cells is achieved by biasing the diffusion of chromosome-associated ParB protein clusters that interact with and alter ParA structures [16, 17, 20, 21]. While ParA filaments have been visualized *in vitro* [16], the structure of ParA clouds has not been clearly established *in vivo* due to the small size of the bacterial cells. Independent of the underlying ParA filament structure, the hydrolysis of ATP has been shown to be a key step for chromosome segregation [16, 20]. An important open question that we study here is how ATP hydrolysis can contribute to biasing ParB cluster diffusion during cell division.

A simple mathematical model that uses specific ParB binding on ParA filament ends can reproduce directed chromosome movement in these cells [22]. In [23] Brownian dynamics simulations of interactions between ParB fibers and ParA polymer bundles showed that ParA hydrolysis-driven depolymerization can be used to bias the diffusion of chromosome-associated ParB. These previous models require ParA depolymerization at the end of the fiber, independent of ParB hydrolysis in order to achieve proper ParB bias. However, it is not clear that this requirement is supported by data [20]. Furthermore, the structure of the ParA bundle has not been established *in vivo*, so it is important to provide a general modeling framework that focuses on the biasing effects of Par ATP-hydrolysis reactions without making too many assumptions about the properties of ParB or ParA

structures. There are two key components that need to be considered for models of ParB translocation: a) ParB protein diffusion, b) ATP hydrolysis of ParA dimers. Further, we make two key simplifying assumptions that allow us to more easily track this problem mathematically. First, we suppose that ParA is arranged into continuous tracks either due to filament formation [16] or continuous ParA nucleoid association [20, 21]. Next, we assume that the ParA ATP hydrolysis due to ParB is a track cutting or "cleaving" reaction, equivalent to 'bridge-burning' in a forward-backward BBM with $p \leq 1$. In previous modeling work of ParA/ParB interactions, the relationships between ATP hydrolysis rates and free diffusion coefficients with effective segregation velocities and diffusion constants could not be obtained analytically. One of the primary contributions of the present work is to provide a simplified modeling framework where we can study the velocity and effective diffusion of the Par segregation machinery.

The models we propose here share a few common features with BBM models, however there are also some fundamental differences between our approach and previous BBM models. First, the analytical results obtained for velocities of BBM models are obtained by extending the periodic hopping model initially proposed by Derrida in 1983 [24] and subsequent extensions in [7, 13]. In these models, a walker moves randomly on a discrete one-track lattice with prescribed probability of burning a discrete part of the track; weak and strong links are typically assumed to be the same length. In contrast, here we take a fundamentally continuous approach for our models. As such, we consider the evolution of probability densities for the position of the cleaving enzyme that acts as a random walker in an infinite continuous track that contains periodically spaced cleaving reaction sites. A cleaving event here can take place independent of the direction of the approach of the random walker (equivalent to the forward-backward BBM). Our models can be studied beyond the asymptotic limits discussed by [5, 9] and our approach for the one-track scenario is tractable enough so that we can obtain explicit solutions for effective bias velocities using mean first passage time calculations. Second, by working in a moving frame of reference, we are able to recast the problem as a renewal-reward stochastic process and thereby gain additional information about the statistics of this process, information that is not available from previous work. Finally, our mean first passage approach can be extended to a model where the random walker hops between two tracks, studied in a future paper [25].

This paper is organized as follows. In Section II, we specify our basic modeling assumptions for the system and present a simple discrete space model for ParA cleaving that permits explicit calculation of relevant velocities, effective diffusion coefficient and corresponding numerical simulations. In section III, we develop a partial differential equation model with continuous space and time variables. This model can also be directly solved to obtain velocities of track cleaving as a function of cleaving rate and enzyme diffusion constant; two important limiting regimes are examined and explicit solutions are derived. Finally, in Section IV we compare the discrete and continuous models.

II. DISCRETE SPACE MODEL

Our modeling strategy is to view the ParB complex as a particle that hops on an infinitely long track with which it can interact and cleave with prescribed rates. We take two modeling approaches, one in which the track is an infinite lattice, for which complex effective bias and diffusion can be computed explicitly. In the second approach, we treat the track as an infinite continuous line on which the ParB complex experiences simple diffusion and cleaving reactions. We start by listing the modeling assumptions that we use for all our modeling approaches and then use the assumptions to develop a discrete space model for Par track cleaving.

i) *ParA arrangement in cells.* The structure of ParA in *C. crescentus* has not been definitively established, so we suppose a simple scenario for the ParA positioning in which the dimers are located along the long axis of a bacterial cell, as diagrammed in Fig.1-(a). We next assume that ParA is arranged into a continuous track along the nucleoid that spans the entire length of a cell. This arrangement of ParA can arise either due to spontaneous filament formation, observed *in vitro* and high resolution *in-vivo* imaging [16], or due to continuous ParA nucleoid association along the length of the cell [20, 21, 26]. A ParA track is necessarily of finite length in a cell, however for our calculations we assume that the ParA track can be represented by a semi-infinite line. The reason for this assumption is that the size of ParB is much smaller than the length of a typical ParA track in cells, and further we are only interested in characteristics of the ParB directed movement away from the edge of the cell.

ii) *ParB arrangement in cells.* ParB proteins assemble onto the bacterial chromosome and form a reactive cluster (referred to as Cleaving Agent or CA in this paper) capable of interacting with a ParA track [16, 26], Fig. 1-(a). We ignore the structure of a chromosome in our model and view the ParB complex as located at a point, corresponding to the center of mass of an ideal spherical ParB cluster.

iii) *Cleaving reaction.* A ParA dimer in the track can react with a ParB protein if the two overlap [16, 20, 21]. In this reaction, ParB hydrolyzes the ParA-associated ATP and breaks the ParA dimer [16, 21], which results in the removal of the dimer from the track (referred to as a 'cleaving reaction' here). Each ParA dimer on the track has length Δx and is assumed to have one site where ParB binders can interact with ParA and cause ATP hydrolysis. In the interest of simplicity, we ignore

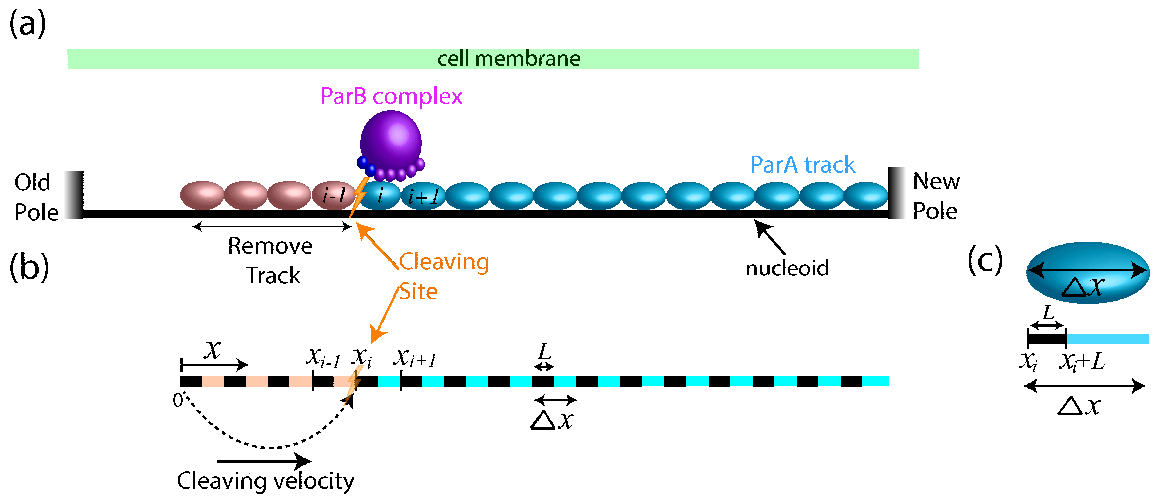

FIG. 1. (Color online) Diagram of the components of the ParA/ParB machinery. a) A track of ParA dimers extends between the two cell poles. Each ParA dimer has one reactive site for the ParB complex, whereas the complex contains several binding sites that can react with a single ParA dimer. The ParB complex has affinity to bind anywhere on the surface of the ParA track however a subset of the ParB binder sites (small spheres) are considered reactive proteins (dark spheres). Reactive ParB binder sites cleave the connections between consecutive ParA dimers. When a dimer i reacts with the ParB complex, the connection between the $i-1$ and i-th site is broken, thus a cleaving reaction occurs. The ParB complex is assumed to stay attached and ahead of the i-th reactive site due to multivalent connections, in a burnt-bridge model fashion. If the i-th ParA dimer reacts, then all the ParA dimers with index $\leq i-1$ are removed from the nucleoid. b) Model diagram for the process. A one-dimensional semi-infinite axis represents the ParA track. The ParB complex and corresponding ParA sites are both represented by uniformly distributed locations of length L (black squares) on the semi-infinite track axis. Only the center of the ParB complex is tracked through a position variable x in the model. $x=0$ corresponds to the most recently cleaved ParA dimer site. c) Diagram comparing a ParA dimer with our model track subunit. The black section of a model ParA track subunit is referred to as reactive site for each dimer and it encapsulates both the ParA binding site and the ParB binders.

the dynamics of each ParB binder and instead assume that all the ParB complex binders and the ParA hydrolysis site can be represented by a *single* ParA track location of finite size that we call a *cleaving site*, corresponding to the black ParA track components diagrammed in Fig. 1-(b)-(c). Thus, the cleaving reaction sites on each ParA dimer are indexed with i and extend from x_i to $x_i + L$ on the semi-infinite track, see Fig. 1-(a)-(b). ATP hydrolysis depends on the density of ParB binder proteins present in the ParB cluster (or equivalently cluster size), supported by observations in [26]. The size of the cluster is implicitly introduced in the model by allowing for variations in the widths $L \leq \Delta x$ of the ParA cleaving sites for each dimer; a larger cleaving site is taken to represent a CA with larger reactive domain (or a ParB complex with more reactive binders). Each cleaving site can then be cleaved by the ParB cluster through a hydrolysis reaction with rate g corresponding to the ATP hydrolysis or cleaving reaction rate per binder.

iv) *ParB/ParA binding.* Besides cleaving, a ParB cluster can also make multivalent binding connections with ParA [16, 20], thus the cluster may have to overcome a significant energy barrier to fully detach from a ParA track. Alternatively, the small spacing between the nucleoid and the cell membrane in *C. crescentus* can force the ParB cluster to stay engaged with a ParA structure, an idea that is supported by confined chamber experiments in [26]. For both scenarios, we assume that a significant amount of energy is required to completely dissociate a ParB cluster from a ParA structure and thus the complex stays associated with the track at all times. This assumption is also aligned with the experimental observations which report continuous tracking of a degrading ParA edge by ParB [16, 17]. In addition, we assume that an attached ParB structure can easily rearrange position on the ParA track, potentially due to weak specific binding affinity between individual ParB binder proteins and ParA sites on the track, in agreement with the observations in [26]. As a result, we suppose that a ParB cluster experiences one dimensional random motion on the surface of the ParA track, with discrete diffusive hopping rate d for a discrete ParA lattice track, or diffusion coefficient D for a continuous ParA track.

v) *Burnt-brdige assumption.* We now specify the assumptions on the positioning of a ParB complex on the ParA track during a hydrolysis event at a cleaving site. Specifically, we make the BBM-type assumption that requires the ParB cluster be found ahead of the cleaved site, so that the CA does not fall off the track following a cleaving reaction, Fig. 1-(a)-(b). A simple possible working hypothesis for this arrangement is that there is a built-in asymmetry in the organization of the sites of a ParB cluster, such that a sequence of ParB multivalent attachments can hold on to the track, while trailing reactive ParB sites actively hydrolyze ATP and break a ParA dimer. As a consequence, the reactive ParB binders can wedge between dimer $i-1$ and i and cause track cleaving at this track juncture; note that we refer to this cleaving event

as occurring at position x_i in the track. We highlight that in this treatment we omit specific ParB binder details, since conclusive data is lacking on the geometry of ParB complex arrangement. Instead, we simply assume that at each cleaving reaction site x_i, the ParB complex remains engaged with the ParA track with position $x > x_i$. We refer to ParB positions with $x > x_i$ as being ahead of the cleaving site and positions with $x < x_i$ as being behind the cleaving site.

vi) *ParA track removal.* Finally, we assume that when a ParB cluster cleaves at x_i, then all the ParA sites with index $\leq i-1$ are also removed from the nucleoid, Fig. 1-(a)-(b). This assumption is based on two potentially related scenarios. First, if the ParA is assembled into a linear actin-like fiber, then this assumption could indicate that a short ParA track with two free ends is unstable and quickly disassembles, a scenario explored in [18]; further, lost free ParA monomers become quickly sequestered at the new cell pole making it less likely for the track to become re-established on the nucleoid once released in the cytoplasm [27]. Second, track removal behind ParB agrees with the observation of ParA-free patches that follow a moving ParB complex in confined artificial assays in [26]. For a single ParA track case that we discuss in this paper, the assumption of ParA removal(or path clearing) during site hydrolysis is not immediately relevant since the burnt-bridge assumption keeps the ParB complex ahead of all cleaved sites at all times. In a multi-track ParA bundle scenario, disconnected ParA tracks behind the last cleaving site could be accessed by the CA traveling on a neighboring continuous track or patch, potentially trapping the CA in isolated ParA islands and creating a loss of directionality. Our ParA patch clearing assumption prevents ParB trapping from occurring and is further explored in another paper [25].

Based on the assumptions above, we develop a simple model of ParB cleaving and hopping on the ParA track. In this section, we use a discrete space assumption for the infinite ParA track. For this purpose, following assumption ii), the cleaving agent is represented as a point particle hopping on a semi-infinite discrete ParA lattice with regular spacing Δx, and we index each ParA cleaving site by j. Cleaving reactions at a particular site can occur with rate g. Each discrete point of the lattice track is a potential cleaving site, so that explicit use of the reactive site length is *not* employed in this setup, but will be explored later in a continuous space model, see diagram in Fig 2-(a)-(b).

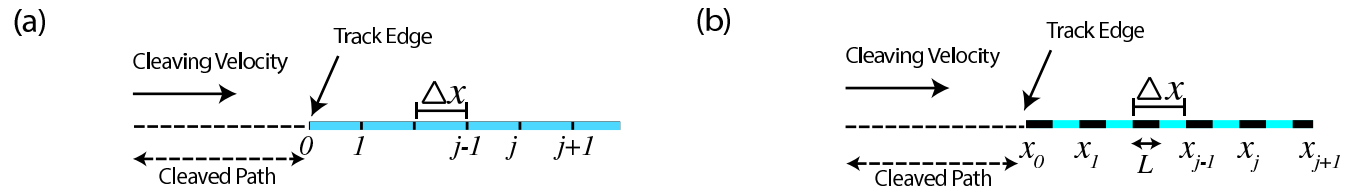

FIG. 2. (Color online) Comparison of discrete vs continuous space models. (a) In the discrete model, we assume the CA is a random walker that hops between discrete space points on a lattice with regular spacing, Δx. Any point on the lattice, j can trigger a cleaving reaction so the width of the reactive region length L is not explicitly included in the model. (b) In the continuous model, the position of the CA, x is a continuous variable. Further, each reactive site has a prescribed non-zero width L(black rectangles), corresponding to regions in space where a cleaving reaction can be triggered with the rate g. In this model, the locations $x_j + L < x < x_{j+1}$ are not reactive and the CA experiences simple diffusion between cleaving sites.

The movement of the CA on the ParA track is affected by two factors: a) cleaving reactions that cause the CA to stay ahead of the ParA cleaving site (assumptions iii) and v)), b) diffusive motion of the CA on the ParA track (assumption iv)). For our model we track a single discrete variable j corresponding to the location on the lattice of the CA. For convenience, we formulate the problem here in a moving frame of reference, so that the 'edge' index $j = 0$ is always located at the most recently cleaved site, and is updated each time a cleaving reaction occurs (i.e., if the next cleaving reaction takes place on site k then $j = k \to j = 0$ and all other index points are shifted by k units). Note that in a relative frame of reference, if the CA is at position indexed by j, the index j is always the location of the CA away from the most recently cleaved site.

Let $p_j(t)$ be the probability of the CA being at site j at time t, then the differential equation for $p_j(t)$ is given by

$$\frac{dp_j}{dt} = d(p_{j-1} - 2p_j + p_{j-1}) - gp_j, \quad j \geq 1 \tag{II.1}$$

$$\frac{dp_0}{dt} = d(p_1 - p_0) + g\sum_{j=1}^{\infty} p_j. \tag{II.2}$$

We highlight two important features of these equations. First, the CA can undergo both diffusion or cleaving at sites j with rates d and g, respectively. Second, since we are in a moving frame of reference, immediately upon a cleavage event at site j, the CA is repositioned to site $j = 0$ (i.e., the coordinate system is shifted). Thus, the reactive terms are added to the p_0 equation to mark the movement of the cleaved sites following each cleaving reaction, reflecting that this is a discrete jump process.

In steady state, the track edge $j = 0$ is moving relative to a fixed frame of reference with the velocity

$$v = g\Delta x \sum_{j=1}^{\infty} j p_j^s, \tag{II.3}$$

where p_j^s is the steady state solution of eq. (II.1)-(II.2). The steady-state equations can be solved explicitly and we obtain the simple expression

$$v = g\Delta x \frac{\lambda}{1-\lambda}, \tag{II.4}$$

where $\lambda < 1$ is a root of the polynomial $\lambda^2 - (2+\alpha)\lambda + 1 = 0$, and $\alpha = g/d$ is a non-dimensional constant.

Two state model: mean first passage time approach. A second approach to this problem is a model in which we examine the cleaving reaction one reaction step at a time. To do so, we distinguish two possible states for all the CA conformations in the cleaving process, one in which the CA is hopping but it has not cleaved, and one in which it has cleaved at some track position. The probability for entering and exiting these two states is then tracked in model equations. For this purpose, we let $p_j(t)$ be the probability that a CA particle located at some point j at a time t has *not* cleaved a track site (note that this p_j is different than the one defined previously). In this case, a particle is able to diffuse on the track and it has a probability per unit time g of exiting this state, if it undergoes a cleaving reaction. Next, we define a new quantity for the process $q_j(t)$ to be the probability that the particle has undergone a cleaving reaction at position j.

For each population of walkers vs. cleavers, we write the system of equations

$$\frac{dp_j}{dt} = d(p_{j-1} - 2p_j + p_{j+1}) - gp_j, \quad j \geq 1, \tag{II.5}$$

$$\frac{dp_0}{dt} = d(p_1 - p_0), \tag{II.6}$$

$$\frac{dq_j}{dt} = gp_j, \quad j > 0. \tag{II.7}$$

In the p_j equation there are two terms, one representing diffusive hops with rate d and the other representing removal of the CA from the not-yet-cleaved state to the cleaved state. The q_j equation has a single reactive term corresponding to cleaving events. Because of the assumption for the cleaving process (assumption iii)) which allows site breaking only between two consecutive dimers, the CA can be absorbed into a site j provided $j \geq 1$. This also means that at the boundary we do not allow cleaving, hence $q_0(t) = 0$ for all time. We start the process with the CA at site $j = 0$ (or at the track edge) so the model initial conditions are that $p_0(0) = 1$, and $p_j(0) = q_j(0) = 0$ for $j > 0$.

It is convenient to write these equations in matrix notation

$$\frac{d\mathbf{p}}{dt} = dW\mathbf{p}, \qquad \frac{d\mathbf{q}}{dt} = gB\mathbf{p}, \tag{II.8}$$

with initial conditions written as $\mathbf{p}(0) = \mathbf{e_0}$ and $\mathbf{q}(0) = 0$.

We are now ready to formulate questions about CA movement. The first is to know the time it takes for the CA to find a cleaving site j. This is a question of the *mean first passage time* of the CA walker cleaving at a particular site j. To calculate these times we must first calculate the total probability of the walker to cleave at some site j (referred to as the splitting probability [28]). The splitting probabilities are defined as $\pi_j = \lim_{t\to\infty} q_j(t) \equiv q_j^\infty$ which can be calculated using vector-matrix notation as

$$\mathbf{q}^\infty = \int_0^\infty \frac{d\mathbf{q}}{dt} dt = gB \int_0^\infty \mathbf{p} dt \tag{II.9}$$

$$= \frac{g}{d} BW^{-1} \int_0^\infty \frac{d\mathbf{p}}{dt} dt = -\alpha BW^{-1}\mathbf{e}_0. \tag{II.10}$$

In addition, the expected splitting time is given by

$$\mathbf{t}^\infty = \boldsymbol{\tau}\mathbf{q}^\infty = \int_0^\infty t\frac{d\mathbf{q}}{dt} dt = \alpha BW^{-1} \int_0^\infty t\frac{d\mathbf{p}}{dt} dt \tag{II.11}$$

$$= -\frac{\alpha}{d} BW^{-2} \int_0^\infty \frac{d\mathbf{p}}{dt} dt = \frac{\alpha}{d} BW^{-2}\mathbf{e}_0. \tag{II.12}$$

Similarly, we obtain $\boldsymbol{\tau}^2\mathbf{q}^\infty = -2\frac{\alpha}{d^2}BW^{-3}\mathbf{e_0}$. Thus, the *conditional mean first passage time* to exit from a particular cleaving site, $\boldsymbol{\tau}$, is given by

$$\boldsymbol{\tau} = \mathbf{t}^\infty./\mathbf{q}^\infty, \tag{II.13}$$

where ./ stands for component-wise division (note that $\boldsymbol{\tau}$ is a vector quantity). We are now able to explicitly calculate the first moments (see Appendix for details) and obtain

$$\langle t\rangle = \sum_j \boldsymbol{\tau}_j = \frac{1}{g\lambda}, \qquad \langle x\rangle = \Delta x \sum_j j\mathbf{q}_j^\infty = \frac{\Delta x}{1-\lambda}, \tag{II.14}$$

where $0 < \lambda < 1$ is a root of the quadratic polynomial $\lambda^2 - (2+\alpha)\lambda + 1 = 0$. The non-dimensional quantity $\alpha = g/d$ reappears here. The parameter α can be interpreted as the effective cleaving rate, measuring the rate of cleaving reactions compared to the rate of diffusive hopping d. Thus, we take d to be $d = \frac{D}{\Delta x^2}$, where D is the diffusion coefficient for the CA particle.

We use the first moments to determine the expected velocity for this system

$$v \equiv \frac{\langle x\rangle}{\langle t\rangle} = \frac{g\Delta x\lambda}{1-\lambda}, \tag{II.15}$$

which is the same as (II.4). Relative to the diffusional velocity $\frac{D}{\Delta x}$, this is

$$\hat{v} = \frac{v\Delta x}{D} = 1 - \lambda, \tag{II.16}$$

with asymptotic expansions for the limiting behavior of the velocity for large and small α as

$$\hat{v} = \frac{v\Delta x}{D} = \sqrt{\alpha} - \frac{\alpha}{2} + O(\alpha^{3/2}), \quad \alpha << 1, \tag{II.17}$$

$$\hat{v} = \frac{v\Delta x}{D} = 1 - \frac{1}{\alpha} + O(\frac{1}{\alpha^2}), \quad \alpha >> 1. \tag{II.18}$$

The velocity we compute here is the velocity of removal of the ParA track due to cleaving, which we refer to as cleaving velocity hereafter, and should not be confused with the velocity of CA movement. A comparison of this calculated velocity with estimates from numerical simulations of the cleaving velocity is shown in Fig 3-(a). The numerical simulation was performed on a discrete track using a Gillespie simulation algorithm [29]. Using a large number of nodes allows us to obtain good statistics for average velocities since finite domain effects are unlikely to affect our computations. Fig. 3-(a) shows excellent agreement between the numerical simulations and the expression in eq. (II.16) when the CA cleaves on the discrete track.

An interesting feature of the cleaving velocities is that the velocity of cleaving does not increase linearly with the non-dimensional cleaving rate α. Instead, the cleaving velocity limits to a constant value for large cleaving rates α. This makes sense since the velocity of cleaving depends not only on how fast each cleaving reaction takes place at a specific site, but also on the time to find cleaving sites. The time to find cleaving sites depends on the diffusive hopping time of the CA between consecutive track sites for large cleaving rates i.e., the velocity is diffusion limited with $v \approx \frac{D}{\Delta x}$ for $\alpha >> 1$. Thus, a very high cleaving rate cannot overcome the fact that it takes time for the CA to travel from one cleaving site to the next. On the other hand, if there are no cleaving reactions on the lattice (i.e., $\alpha = 0$), then the ParA edge cleaving velocity is also zero with no track edge movement, as expected.

A. Renewal-reward approach and higher moments

The mean first passage time analysis in the previous section allows us to calculate how fast, on average, the track is cleaved. While this velocity is an important quantity, it does not tell us much about other statistics of the CA, such as higher moments for CA displacement. For example, higher order statistics can be used to define the effective diffusion coefficient for the CA. There have been previous definitions of such quantities in [13]. In this section, we provide an analysis that allows us to compute the CA effective diffusion coefficient as a function of the cleaving rates.

For this analysis, it is convenient to write a model that tracks the position of the CA as it transitions between consecutive cleaving events. For this purpose, we define $P_k(i,t)$ as the probability of the k^{th} track-cleaving event taking place at position $i\Delta x$, in a fixed frame of reference, at time t (note that the $k-1$ cleaving event takes place at position with index $j < i$). Then,

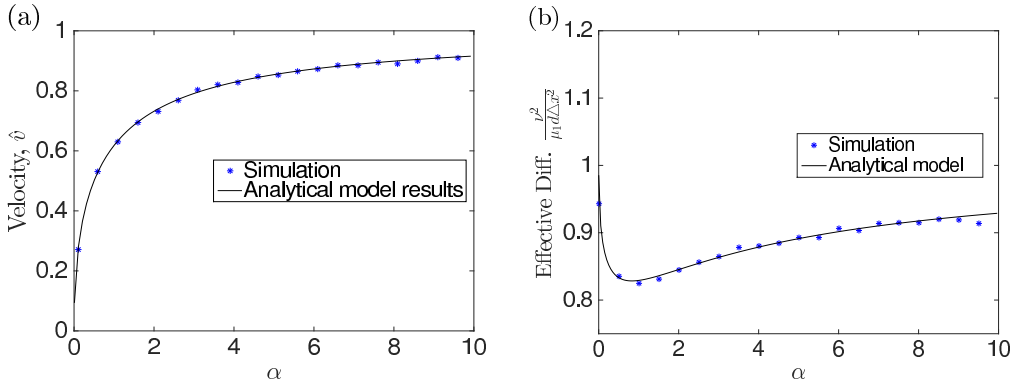

FIG. 3. (Color online) Discrete model results. a) Comparison between non-dimensional analytical velocity results in eq. (II.16) and simulation results. Numerical simulations were performed using a Gillespie algorithm for a discrete lattice track. Numerical results are in excellent agreement with calculated velocities. b) Effective diffusion coefficient, $\frac{\nu^2}{\mu_1 d\Delta x^2}$. The analytical effective diffusion is computed using eq.(II.32) (solid line). The effective diffusion is compared with stochastic simulation diffusion, $\frac{\hat{\sigma}^2}{\mu_1 d\Delta x^2} = \frac{1}{d\mu_1 \Delta x} var(n - \frac{\bar{n}}{\bar{t_n}} t_n)$, where n is the amount of cleaved track during t_n interval, obtained from Gillespie simulations.

$P_k(i,t)$ satisfies the time-continuous map

$$P_k(i,t) = \int_{-\infty}^{t} \sum_{j=-\infty}^{i-1} P_{k-1}(j,s) \frac{dq_{i-j}}{dt} ds \tag{II.19}$$

$$= g \int_{-\infty}^{t} \sum_{j=-\infty}^{i-1} P_{k-1}(j,s) p_{i-j}(t-s) ds. \tag{II.20}$$

The probabilities p, q are defined as in the previous section as the one-cleavage step probabilities, and obey the eq. (II.5)-(II.7). The mapping tracks the transition of the CA between consecutive cleaving events; the summation of probabilities indicates that a CA can reach and cleave at position i, in a fixed frame of reference, from any track position $j \leq i-1$. In eq. (II.20), we use the definition of dq/dt from Sect. II, with $i-j$ being the size of the cleavage step. These probabilities are then integrated over time to account for all possible times when cleaving can occur for this process.

Casting the problem in terms of this one-step process has several advantages, the primary one being that we can compute higher order moments for cleaving distances of the CA. We define the first moments in both independent variables for this process as

$$Mx_k^1 = \int_{-\infty}^{\infty} \sum_{i=-\infty}^{\infty} i P_k(i,t) dt, \quad Mt_k^1 = \int_{-\infty}^{\infty} \sum_{i=-\infty}^{\infty} t P_k(i,t) dt. \tag{II.21}$$

Upon substitution of eq. (II.20), the respective moments, Mx_k^1, Mt_k^1 are found to obey the recursive relations

$$Mx_k^1 = Mx_{k-1}^1 + Mx_{k-1}^0 \langle x \rangle, \quad \text{where} \quad \langle x \rangle = \sum_{i=1}^{\infty} \int_0^{\infty} i \frac{dq_i}{dt} dt, \tag{II.22}$$

and since $Mx_{k-1}^0 = \int_{-\infty}^{\infty} \sum_{i=-\infty}^{\infty} P_{k-1}(i,t) dt = 1$, the mapping simplifies to

$$Mx_k^1 = Mx_{k-1}^1 + \langle x \rangle, \tag{II.23}$$

and similarly we obtain

$$Mt_k^1 = Mt_{k-1}^1 + \langle t \rangle. \tag{II.24}$$

These calculations indicate that the moments for this process are additive and can be obtained recursively; this feature is extremely useful in computing higher moments from the process given that we already know $\langle x \rangle, \langle t \rangle$ from the discrete model in the previous section. The second moments follow in the same way (see Appendix), for example

$$Mx_k^2 = Mx_{k-1}^2 + 2Mx_{k-1}^1\langle x\rangle + \langle x^2\rangle, \quad \text{where} \quad \langle x^2\rangle = \Delta x^2 \sum_{i=1}^{\infty}\int_0^{\infty} i^2 \frac{dq_i}{dt}dt. \tag{II.25}$$

In a similar way, one calculates equations for the second order cross-moments (see Appendix). For example

$$Mxt_k = Mxt_{k-1} + \langle x\rangle Mt_{k-1}^1 + \langle t\rangle Mx_{k-1}^1 + \langle xt\rangle, \tag{II.26}$$

where we define

$$Mxt_k = \int_{-\infty}^{\infty}\sum_{i=-\infty}^{\infty} itP_k(i,t)dt, \quad \langle xt\rangle = \sum_{i=1}^{\infty}\int_0^{\infty} it\frac{dq}{dt}dt. \tag{II.27}$$

Framing the model in this way allows us to think of random site cleaving through a stochastic process. Specifically, we define the continuous-time stochastic process $\{x(t), t \in [0,\infty]\}$ with $x(t)$ denoting the position of the most recent cleavage event at time t. This process is regenerative since there is a random time t_k, corresponding to the time of the k^{th} cleaving reaction with the property that the cleavage distance, $x(t_k) - x(t_{k-1})$, is independent of previous cleavage distances. This is because, immediately following a cleavage event, the underlying diffusion process starts anew until the next cleaving event. Next, we define the random variables $T_k = t_k - t_{k-1}$ with $t_0 = 0$ corresponding to times between cleaving events. The sequence $\{T_k\}$ defines a renewal process with $0 < E(T_1) < \infty$ provided $\alpha > 0$. A reward structure can be imposed on this regenerative process. We let $X_k = x_k - x_{k-1}$ corresponding to the distance between cleaving positions; $X(t)$ is defined to be the cumulative reward earned up to time t and the process $\{X(t), t \geq 0\}$ is called a renewal-reward process [30]. The probability densities for these random variables are described by the recursion in eq. (II.20).

An important feature of renewal-reward processes is that the long-run behavior of the process can be determined in terms of the behavior of the process during a *single* regeneration cycle [30]. Further, the long-run behavior for this process is known by means of a central limit theorem (CLT)(see [31] for details), which states that for large t, the process $X(t)$ is approximately normally distributed with mean ηt and variance $\nu^2 t/\mu_1$, where $\mu_1 = \langle T_1\rangle$, $\eta = \langle X_1\rangle/\langle T_1\rangle$ and $\nu^2 = \langle (X_1 - \eta T_1)^2\rangle$ are mean and variance quantities that are computed from a single step of the process. The term η is exactly the average cleaving velocity, so we have that $\eta = v$. The quantity ν^2 is the variance for this process, and it depends on both the reward random variable and renewal cycle random variable. Based on this limiting distribution, we define the dispersion for our process to be

$$\nu^2 = \langle (X_1 - v\,T_1)^2\rangle \tag{II.28}$$

$$= \langle x^2\rangle - 2v\langle xt\rangle + v^2\langle t^2\rangle. \tag{II.29}$$

where we have used that $\langle X_1^2\rangle = Mx_1^2 = \langle x^2\rangle$ (eq.II.25), $\langle XT\rangle = Mxt_1 = \langle xt\rangle$ (eq. II.26), and $\langle T_1^2\rangle = Mt_1^2 = \langle t^2\rangle$.

We can compute ν^2 using the second moments which are obtained explicitly and are

$$\langle t^2\rangle = \frac{2}{g^2\lambda^2}\frac{1+\lambda^2}{1+\lambda}, \qquad \langle x^2\rangle = \Delta x^2\frac{1+\lambda}{(1-\lambda)^2}, \qquad \langle xt\rangle = \frac{\Delta x}{g}\frac{\lambda^2+\lambda+1}{\lambda(1-\lambda^2)}. \tag{II.30}$$

which yields the simple expression for ν^2

$$\nu^2 = \Delta x^2\frac{1+\lambda^2}{(1-\lambda)^2(1+\lambda)}. \tag{II.31}$$

The quantity ν^2/μ_1 is given by

$$\frac{\nu^2}{\mu_1} = d\Delta x^2\frac{1+\lambda^2}{1+\lambda}, \tag{II.32}$$

and is the effective diffusion constant of the CA. Asymptotic expansions readily reveal the limiting behaviors of these quantities

$$\frac{\nu^2}{\Delta x^2} = \frac{1}{\alpha} + O(\alpha^{-\frac{1}{2}}), \quad \frac{\nu^2}{\mu_1 d\Delta x^2} = 1 - \frac{1}{2}\sqrt{\alpha} + O(\alpha), \tag{II.33}$$

for $\alpha << 1$, and

$$\frac{\nu^2}{\Delta x^2} = 1 + \frac{1}{\alpha}O(\alpha^{-2}), \quad \frac{\nu^2}{\mu_1 d\Delta x^2} = 1 - \frac{1}{\alpha} + O(\alpha^{-2}), \tag{II.34}$$

for $\alpha >> 1$. A comparison between the effective diffusion $\frac{\nu^2}{\mu_1 d\Delta x^2}$ and the diffusion obtained from stochastic Gillespie simulations of this process, $\frac{1}{\mu_1 d\Delta x^2}\hat{\sigma}^2 = \frac{1}{\mu_1 d\Delta x^2} var(n - \frac{\bar{n}}{\bar{t}_n} t_n)$, where n is the amount of cleaved track in a t_n interval, is shown in Fig. 3-(b). The predicted effective diffusion from our model is in excellent agreement with the simulation statistics. The effective diffusion also shows some interesting properties. When $\alpha = 0$ the effective diffusion becomes $\frac{\nu}{\mu_1 d\Delta x} = \frac{\nu}{\mu_1 D} = 1$ or $\frac{\nu}{\mu_1} = D$ corresponding to the free diffusion coefficient of the CA, which is expected since D is the diffusion coefficient corresponding to reaction-free regimes. For $\alpha \to \infty$, the effective diffusion also limits to D, the free diffusion coefficient; one way to interpret this is that in the fast cleaving regime the CA the reactions become almost instantaneous thus the CA spends no additional time in cleaving reactions as it diffuses between cleaving sites. In an intermediate α regime, interestingly we observe that the effective diffusion coefficient of the CA is smaller than free diffusion coefficient D (approx. 20% reduction), and this is most likely connected to a slow down due to time spent for each cleaving reaction in this α range. This range of lowered diffusion is an interesting result from our model that we discuss later.

III. A CONTINUOUS SPACE MODEL WITH FINITE SIZE CLEAVING SITES

In this section, we let the position of the CA be a continuous variable, generalizing the work of [5, 9] for autocatalytic reaction waves and collagenase cleaving. With a continuous position assumption, the cleavage model can be described in terms of differential equations which can be analyzed to compute relevant properties of the CA.

For this second model, we again use a moving frame of reference with position $x = 0$ located at the leftmost edge of the one-dimensional lattice, corresponding to the edge of the last cleaved site. Thus, as in the discrete space model, we follow the evolution of a continuous position variable, x that gives the distance between the polymer track edge and the center of the CA, as shown in Fig 2-(b). The CA diffuses on the ParA track and also reacts with the track at specific cleaving sites indexed by $i = 1, 2, 3 \ldots$. We assume a regular distribution of cleaving sites with $x_{i+1} - x_i = \Delta x$, however, in contrast with the discrete model, on a particular ParA dimer the cleaving site extends from x_j to $x_i + L$, so the distance between consecutive sites is $\Delta x - L$. The site positions are given by the relation $x_i = i\Delta x$.

We write a differential Chapman-Kolmogorov (CK) equation [32] to describe the evolution of the probability density, $p(x,t)$, of finding the CA at position x at time t

$$\frac{\partial p(x,t)}{\partial t} = D\frac{\partial^2 p(x,t)}{\partial x^2} + \int_{-\infty}^{\infty} dz[W(x|z)p(z,t) - W(z|x)p(x,t)]. \tag{III.1}$$

The two components in this model are the diffusive term with diffusion constant, D, and the cleaving reaction jump terms. An important idea to highlight here is that the reactions cause the CA to move on the track each time a cleaving reaction occurs due to the moving frame of reference; every time a reaction occurs the zero position is moved to the most recently cleaved site, Fig 1. The reaction terms in the CK are given by the time independent jump transition probabilities $W(x|y)$ that depend on the cleaving reaction rate function $\phi(x)$, which is in turn defined as

$$\phi(x) = \frac{\gamma}{L}\chi(x) = \begin{cases} \frac{\gamma}{L} & \text{if } 0 \le x \le L \\ 0 & \text{otherwise,} \end{cases} \tag{III.2}$$

where γ is the absorption rate into a track cleaving site and $\chi(x)$ is an indicator function. For simplicity, we assume that all the cleaving reaction rates are the same, γ for all i positions on the track.

We obtain the following CK equation that describes the evolution of the conditional probability density, $p(x,t)$ of finding the CA at position x at time t

$$\frac{\partial p(x,t)}{\partial t} = D\frac{\partial^2 p(x,t)}{\partial x^2} + \phi(x)\sum_{i=1}^{\infty} p(x + x_i, t) - \sum_{i=1}^{\infty} \phi(x - x_i)p(x,t). \tag{III.3}$$

The resulting reactive terms in the CK are dictated by the moving frame of reference in this model and can be interpreted as follows. In the moving frame, each cleaving reaction results in the instantaneous movement of the most recent cleavage site, x_i, to the zero point, thus the x position of the CA moves to position $x - x_i$. The the sink terms represent cleavage at position x_i and the source term represent repositioning of the CA in the moving frame of reference.

The boundary conditions are $p'(0,t) = 0$ and $\lim_{x\to\infty} p(x,t) = 0$. The reflective condition at the $x = 0$ boundary is imposed to contain the complex on the ParA track, since we assume that the CA has high non-specific biding affinity for the ParA track. Note that the terms in eq. (III.3) are such that there are no cleavage reactions in the interval $0 < x < L$.

The cleaving velocity of the track by the complex is calculated as the net sum of all the possible cleaving steps (or reactions) catalyzed by the CA on the ParA track. Accordingly, the velocity is

$$v \equiv \int \sum_{i=1}^{\infty} \phi(x - x_i) p_s(x) dx = \frac{\gamma}{L} \int \sum_{i=1}^{\infty} x_i \chi(x - x_i) p_s(x) dx, \tag{III.4}$$

where $p_s(x)$ is the steady state distribution of eq. (III.3), marking the steady state distribution of the CA position relative to the track. We note that this velocity is the track shortening velocity caused by a diffusing hydrolysis-inducing element that can react with the track at arbitrary sites, not to be confused with the velocity of the CA itself. The steady state distribution solutions of the CA position, $p_s(x)$, can be readily obtained from eq. (III.3) using the assumed rate functions, $\phi(x)$. The main steps of the steady-state calculations for this model are given in the Appendix.

An explicit expression for v as a function of the cleaving rate and cleaving site length can be readily obtained and its derivation is outlined in the Appendix. As in the discrete case, we use the rescaling $\hat{v} = v\frac{\Delta x}{D}$, $\alpha = \frac{\gamma \Delta x}{D}$ and $k = \frac{L}{\Delta x}$ corresponding to non-dimensional velocity, cleaving rate and cleaving site length, respectively. The velocity in two limiting cases of reaction site lengths can be readily computed to be

$$\frac{v\Delta x}{D} = \alpha \frac{2\lambda}{1 - \lambda^2}, \quad L \to 0, \tag{III.5}$$

where $\lambda < 1$ satisfies $\lambda^2 - (2 + \alpha)\lambda + 1 = 0$, and

$$\frac{v\Delta x}{D} = \frac{2\sqrt{\alpha}}{2 + \sqrt{\alpha}}, \quad L \to \Delta x. \tag{III.6}$$

We show a plot of the rescaled velocity $\hat{v} = v\frac{\Delta x}{D}$ as a function of the parameter $\alpha = \frac{\gamma \Delta x}{D}$ for several site lengths $k = \frac{L}{\Delta x} > 0$ in Fig. 4-(a). The velocity solutions show ordering for varying cleaving site lengths, as measured by the non-dimensional parameter k. Moreover, velocity ordering is particularly prominent for small α, however as $\alpha \to \infty$, all the velocities limit to the same constant value which corresponds to the diffusive transition velocity across Δx segments, since the CA cannot move faster than the diffusive rate, $v_D = D/\Delta x$. The cleaving velocity responses can be readily seen with the help of asymptotic expansions in two different α regimes for the non-dimensional velocity expression

$$\hat{v} = \frac{v\Delta x}{D} = \sqrt{\alpha} - \frac{1}{2} k\alpha + O(\alpha^{3/2}), \quad \alpha << 1, \quad 0 < k \leq 1, \tag{III.7}$$

$$\hat{v} = \frac{v\Delta x}{D} = 2 - 4\sqrt{\frac{k}{\alpha}} + 8\frac{k}{\alpha} + O\left(\alpha^{-3/2}\right), \quad \alpha >> 1, \quad 0 < k \leq 1. \tag{III.8}$$

and for $k = 0$

$$\hat{v} = \frac{v\Delta x}{D} = \sqrt{\alpha} - \frac{1}{8}\alpha^{3/2} + O(\alpha^{5/2}), \quad \alpha << 1, \tag{III.9}$$

$$\hat{v} = \frac{v\Delta x}{D} = 2 - 4\frac{1}{\alpha} + 12\frac{1}{\alpha^2} + O(\alpha^{-3}), \quad \alpha >> 1. \tag{III.10}$$

All the expansions have the same limiting behavior with α given by $\lim_{\alpha \to 0} \hat{v} = 0$ and $\lim_{\alpha \to \infty} \hat{v} = 2$, respectively. The reason that $\hat{v}$ limits to the same constant value, independent of k, as $\alpha \to \infty$, can be understood by noting that each cleaving event can contribute at most Δx removal from the track independent of k in this model (i.e., a ParB can at most remove a single dimer). On the other hand, when $\alpha = 0$, there are no cleaving events and the system is necessarily static, since the track cannot be cleaved. These model results are in agreement with corresponding BBM model velocities results [7, 9]. The steady-state probabilities versus the non-dimensional position variable $y = x/\Delta x$ in Fig. 4-(b) show that the CA is more likely to be found near to the edge of the lattice as the cleaving rate increases. These results agree with what we expect for this process, since a faster cleaving rate should not give the CA enough time to diffuse far from the edge of the track between consecutive cleaving events.

Next we study two limiting cases for this model, where expected velocities and many other movement statistics can be explicitly obtained.

A. Point cleaving rates: the $L \to 0$ limit

We start with a special case for the cleaving rate functions $\phi(x)$ in the limit where the length of the reactive site becomes infinitely small, corresponding to $L \to 0$. This rate function corresponds to the idealized case in which the target for CA

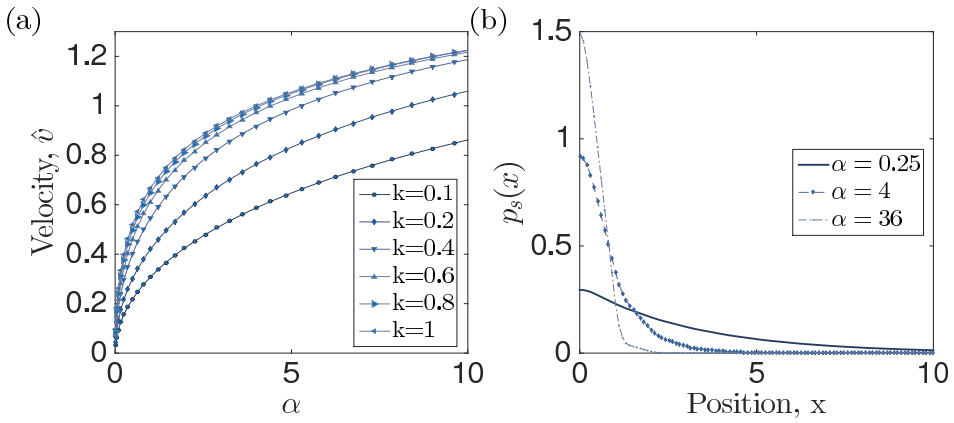

FIG. 4. (Color online) Continuous model results. (a) Non-dimensional velocity, $\hat{v}$ plotted as a function of α with varying trap length measured by the non-dimensional parameter k. For high cleaving rates α velocities limit to the same constant values independent of the size of the cleaving sites on the track. If cleaving does not occur i.e., $\alpha = 0$, then the cleaving velocity is zero and the CA is not reacting with the track. (b) Steady-state probability density solution, $p_s(y)$ with $\Delta x = 1$ and $k = 0.4$, $\hat{\alpha} = 0.5, 2, 6$. The peaks on the distributions show that the CA is more likely to be found at the edge of the track if the cleaving rate increases, since there is less time to diffuse away from $x = 0$ in each reaction cycle.

cleaving on the ParA track is infinitesimally small, however, the rate of hydrolysis once there is sufficiently high to make up for the diminished target size; for this reason we refer to this scenario as a point cleaving rate model. In this limit we have

$$\frac{\partial p}{\partial t} = D\frac{\partial^2 p}{\partial x^2} - \gamma \sum_{i=1}^{\infty} \delta(x - x_i)p + \gamma\delta(x) \sum_{i=1}^{\infty} p(x + x_i). \tag{III.11}$$

For this problem we can find the velocity directly since the model equation is relatively easy to solve in steady state, so the velocity is given by

$$\frac{v\Delta x}{D} = \alpha \frac{2\lambda}{1 - \lambda^2}, \tag{III.12}$$

where λ satisfies the characteristic equation $\lambda^2 - (\alpha+2)\lambda + 1 = 0$. We note that the expression obtained here is the same as the one obtained in the limit of $L \to 0$ cleaving site lengths in the continuous space model. Further, the characteristic polynomial used to determine λ here is similar to the one for the discrete space model, indicating similarities between the two models; we discuss this in more detail later. Asymptotic formulae for the velocity can be readily obtained

$$\frac{v\Delta x}{D} = \hat{v} = \sqrt{\alpha} - \frac{1}{8}\alpha^{\frac{3}{2}} + O(\alpha^{\frac{5}{2}}), \quad \alpha << 1, \tag{III.13}$$

$$\frac{v\Delta x}{D} = \hat{v} = 2 - \frac{4}{\alpha} + O(\alpha^{-2}), \quad \alpha >> 1. \tag{III.14}$$

As expected, the velocity obtained in this limit case is in full agreement with the continuous model velocity as $L \to 0$, indicating that the $\delta(x)$ rate function approach is appropriate for this limit case.

Two state model: mean first passage approach. Instead of solving the PDE model at steady-state we can compute times for cleaving events and the expected position where the cleaving takes place. The ratio between expected cleaving distance and the expected time it takes to exit through the cleaving site is the expected velocity for the process; this is a *mean first passage time* problem, similar to the discrete model case. To apply this approach, we present a new modeling approach that allows us to easily leverage mean exit time calculations. A simple calculation along these lines was given in [9], but only for two special BBM limiting cases $\alpha \to 0$ and $\alpha \to \infty$. Here we demonstrate a more general approach that permits direct velocity calculations for varying α regimes. We expect that this approach can easily extend to other BBM type models. Furthermore, in another paper [25] we show that the mean first passage approach can be applied to a more general model where the CA can move along two parallel tracks.

For the mean first passage approach we write the following system of differential equations following the same ideas of the

discrete model; the quantities p, q are now given by the following system of differential equations

$$\frac{\partial p}{\partial t} = D\frac{\partial^2 p}{\partial x^2} - \gamma \sum_{i=1}^{\infty} \delta(x - x_i)p, \tag{III.15}$$

$$\frac{dq_i}{dt} = \gamma p(x_i). \tag{III.16}$$

where $\delta(x - x_i)$ specifies the rate of cleaving at position x_i. Similar to the previous section, we impose reflecting boundary condition at $x = 0$, $\frac{\partial p(x,t')}{\partial x}|_{x=0} = 0$ for the partial differential equation in the state p; this condition prevents the CA from leaving the track due to diffusive flux. We obtain three relevant equations for the exit probabilities and times (see Appendix for more details) as follows

$$D\frac{d^2\pi_i}{dx^2} - \gamma \sum_{j>0} \delta(x - x_j)\pi_i = -\gamma\delta(x - x_i), \tag{III.17}$$

$$D\frac{d^2 G_i}{dx^2} - \gamma \sum_{j>0} \delta(x - x_j)G_i = -\pi_i(x), \tag{III.18}$$

$$D\frac{d^2 T_i^2}{dx^2} - \gamma \sum_{j>0} \delta(x - x_j)T_i^2 = -2G_i(x), \tag{III.19}$$

where the quantity $\pi_i(x)$ gives the probability of the CA exiting through site x_i given that the starting position is x, $T_i(x)$ is the corresponding conditional mean first passage time (MFPT), and $G_i = T_i(x)\pi_i(x)$.

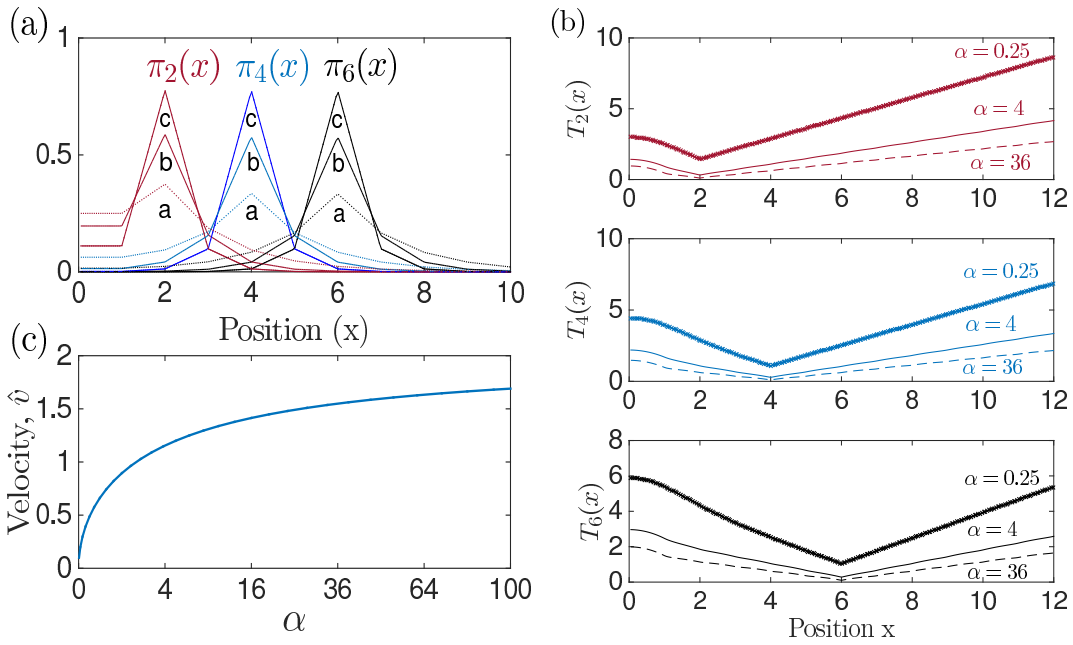

FIG. 5. (Color online) Model results for the point-cleaving rate limit. (a) Exit probabilities, $\pi_i(x)$ with $\Delta x = 1$, $i = 2, 4, 6$ and three cases of cleaving rates $\alpha =$ a) 0.25, b) 4, c) 36. The probabilities peak at the index site i with higher probabilities occurring for higher cleaving rates α. (b) Mean first passage times, $T_i(x)$ for three exit sites indexed $i = 2, 4, 6$, $\alpha = 0.25, 4, 36$, and $\Delta x = 1$. The mean exit times are the lowest at the exit site positions $x = i$. (c) The non-dimensional track cleaving velocity, $\hat{v}$ is shown as a function of the parameter α. The velocity shows qualitatively similar saturating behavior to the discrete model velocities.

Plots of representative solutions for $\pi_i(x)$ and $T_i(x)$ are given in Fig. 5-(a)-(b). The exit probabilities, $\pi_i(x)$ peak when the initial positions are close to x_i, indicating that the likelihood of exiting through a particular site increases if the process is started

with positions close to x_i. Also, we note that the likelihood of exiting (or cleaving) at a site increases as the cleaving rate α increases, as should be expected. On the other hand, the mean exit times, $T_i(x)$ dip around the cleaving point position x_i, since the CA is almost instantaneously absorbed at the site if it starts close enough to it. As expected, the exit times increase with increasing distance of the initial position x from the cleaved site i. On the other hand, as the non-dimensional parameter α is increased, the relative cleaving rate is also increased, which results in an overall shortening of exit times for all starting positions.

The hitting probabilities and the MFPT can be used to obtain the following moments for the problem

$$\langle t \rangle = \sum_{i>0} G_i(0), \qquad \langle t^2 \rangle = \sum_{i>0} T_i^2(0), \tag{III.20}$$

and

$$\langle x \rangle = \Delta x \sum_{i>0} i\pi_i(0), \qquad \langle x^2 \rangle = \Delta x^2 \sum_{i>0} i^2\pi_i(0), \qquad \langle xt \rangle = \Delta x \sum_{i>0} iG_i(0). \tag{III.21}$$

Upon solving the above equations, the x moments can be explicitly computed and they are

$$\langle x \rangle = \frac{\Delta x}{1-\lambda}, \qquad \langle x^2 \rangle = \Delta x^2 \frac{\lambda+1}{(1-\lambda)^2}, \tag{III.22}$$

which are exactly the same as the moments we derived for the discrete space problem. To find $\langle t \rangle$, we note that $\langle t \rangle = G(0)$, where $G = \sum_i G_i$ satisfies

$$D\frac{d^2G}{dx^2} - \gamma \sum_{j>0} \delta(x - x_j)G = -1, \tag{III.23}$$

since $\sum_i \pi_i(x) = 1$. Then, we obtain

$$\langle t \rangle = \frac{(1+\lambda)\Delta x}{2\gamma\lambda}. \tag{III.24}$$

Finally, average cleaving velocities are calculated using the following expression

$$v = \frac{\langle x \rangle}{\langle t \rangle} = \frac{2\gamma\lambda}{1-\lambda^2}, \tag{III.25}$$

which agrees with the equation (III.12). Using the same non-dimensionalization as before we obtain

$$\hat{v} = \alpha \frac{2\lambda}{1-\lambda^2}. \tag{III.26}$$

The cleaving velocity, $\hat{v}$, as a function of the non-dimensional parameter $\alpha = \frac{\gamma\Delta x}{D}$ for this model is given in Fig. 5-(c). As before, we see that the effective track cleaving velocity saturates as the relative hydrolysis rate, measured by α, is increased, as we saw in the previous section. This indicates that the model we consider here gives qualitatively similar results to the previous PDE model.

The other moments can also be obtained after some work (see Appendix) and we have

$$\langle t^2 \rangle = \frac{\triangle x^2}{12\gamma^2} \frac{\lambda^4 + 2\lambda^3 + 30\lambda^2 + 2\lambda + 13}{\lambda(1+\lambda)}, \quad \langle xt \rangle = \frac{\Delta x^2}{6\gamma} \frac{2\lambda^3 - 11\lambda^2 - 8\lambda - 3}{\lambda(1-\lambda^2)}. \tag{III.27}$$

Finally, we calculate the variance of the renewal-reward process to be

$$\nu^2 = \langle x^2 \rangle - 2v\langle xt \rangle + v^2\langle t^2 \rangle \tag{III.28}$$

$$= \frac{2\Delta x^2}{3}\Big(\frac{\lambda^4 + 2\lambda^3 + 6\lambda^2 + 2\lambda + 1}{(1-\lambda)^2(1+\lambda)^3}\Big), \tag{III.29}$$

and the effective diffusion coefficient to be

$$\frac{\nu^2}{\mu_1}\frac{1}{D} = \frac{4}{3}\left(1 - 2\frac{\lambda(\lambda^2+1)}{(1+\lambda)^4}\right). \tag{III.30}$$

Asymptotic expansions give

$$\frac{\nu^2}{\mu_1}\frac{1}{D} = 1 + \frac{1}{48}\alpha^2 + O(\alpha^3), \tag{III.31}$$

for $\alpha \ll 1$ and

$$\frac{\nu^2}{\mu_1}\frac{1}{D} = \frac{4}{3} - \frac{8}{3}\frac{1}{\alpha} + O(\alpha^{-2}), \tag{III.32}$$

for $\alpha \gg 1$.

B. Continuous cleaving: the $L \to \Delta x$ limit

In this limit, the model becomes the continuous binding model,

$$Dp_{xx} - \frac{\gamma}{\Delta x}p = 0, \qquad \Delta x < x < \infty, \tag{III.33}$$

and

$$Dp_{xx} + \frac{\gamma}{\Delta x}\sum_{i=1}^{\infty} p(x + i\Delta x) = 0, \qquad 0 < x < \Delta x, \tag{III.34}$$

with boundary condition $p_x = 0$ at $x = 0$. Explicit solutions can be easily obtained in this case for the steady state distributions. The velocity is then found to be

$$v = \frac{\gamma}{\Delta x}\int_0^{\Delta x}\sum_{i=1}^{\infty} x_i p(x + x_i)dx = \frac{\gamma}{\beta\Delta x(1 + \frac{1}{2}\beta\Delta x)}. \tag{III.35}$$

where $\beta = \sqrt{\frac{\gamma}{\Delta x D}} = \sqrt{\frac{\alpha}{\Delta x}}$. In non-dimensional terms, we obtain a simple expression for the velocities in this limiting case

$$\hat{v} = \frac{v\Delta x}{D} = \frac{2\sqrt{\alpha}}{2 + \sqrt{\alpha}}. \tag{III.36}$$

Asymptotic expansions give

$$\frac{v\Delta x}{D} = \sqrt{\alpha} - \frac{1}{2}\alpha + O(\alpha^{3/2}), \quad \alpha << 1 \tag{III.37}$$

$$\frac{v\Delta x}{D} = 2 - 4\frac{1}{\sqrt{\alpha}} + 8\frac{1}{\alpha} + O(\alpha^{-3/2}), \quad \alpha >> 1. \tag{III.38}$$

These results are in agreement with the calculations of the full continuous model velocity in the limit $\lim_{k\to 0}\hat{v}$ (see Appendix).

IV. COMPARISON OF MODELING APPROACHES

We have discussed two modeling approaches for CA track cleaving; for both cases we took a moving frame approach coupled with a two state model to compute average velocities and movement statistics. An important question is to examine in what limit the two modeling approaches correspond to one another. The non-dimensional parameter α is useful for this purpose. Recall that for the discrete space case, velocities were expressed in terms of λ, which is the root $\lambda < 1$ of the characteristic polynomial $\lambda^2 - (2 + \alpha)\lambda + 1 = 0$ with $\alpha = g\Delta x^2/D$. On the other hand, for the continuous space case, solutions were expressed in terms of the quantity $\lambda < 1$ that satisfies the characteristic polynomial $\lambda^2 - [2\cosh(\hat{\alpha}k) + (1 - k)\hat{\alpha}\sinh(\hat{\alpha}k)]\lambda + 1 = 0$ with $\alpha = \gamma\Delta x/D$. The intuitive limit where the continuous and discrete model should agree is the case where $L \to 0$ or $k \to 0$. Indeed, in the limit $k \to 0$, the characteristic polynomial for the continuous model reduces to the familiar discrete polynomial $\lambda^2 - (2 + \alpha)\lambda + 1 = 0$, which is equivalent to the discrete model provided we define α appropriately for the continuous case. Thus, to appropriately compare the discrete and continuous model results it is reasonable to set $\gamma = g\Delta x$. Using this γ we have a uniform α parameter definition for all our results so that proper comparisons can be made.

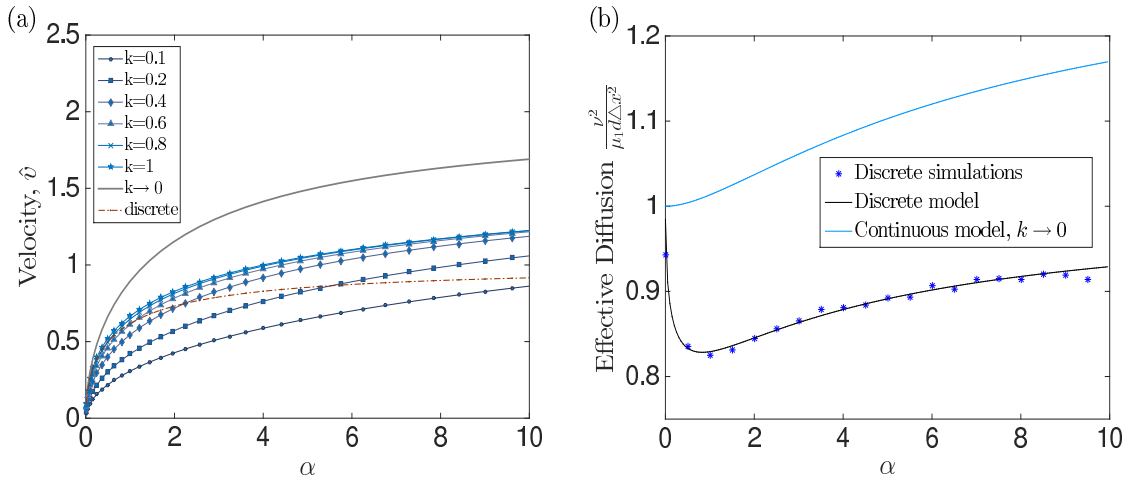

FIG. 6. (Color online) Comparison of all model results. a) Plot comparing all the average velocity results for each model. b) Comparison of the effective diffusion constant for the discrete model and the continuous model with point cleaving rates $L \to 0$.

Plots of the velocities and effective diffusion coefficients for the two models (continuous and discrete) plotted as a function of α are shown in Fig. 6.

In Fig. 6-(a) we see that the velocities for the two models and the different parameter choices show the same qualitative behavior, namely that $v \to 0$ as $\alpha \to 0$ and that v approaches some constant value as $\alpha \to \infty$. The constant approached by the velocity of the discrete and continuous models is different; in the continuous model, $v \to 2$ for any k (including $k \to 0$), whereas in the discrete model $v \to 1$. The discrepancy is due to the fact that in the limit of large α, the reaction at the first reactive site on the track is almost instantaneous so that the velocity is determined entirely by the time it takes the CA to reach the first site. For the continuous model, the expected time to diffuse a distance Δx is the diffusive rate $\frac{\Delta x^2}{2D}$. On the other hand, for the discrete model, since the movement is by a Poisson process with rate d, the expected time to reach the first site is $1/d = \frac{\Delta x^2}{D}$, which is twice the amount of time for the continuous model. This discrepancy is not apparent in the case where α is small since for slow reactions, diffusion on a discrete lattice and the continuous line are the same. This point is also demonstrated by the plots in Fig.6-(b), where it is seen that the effective diffusion coefficients for the discrete and continuous model with point cleaving rates agree at $\alpha \approx 0$. The qualitative behavior of the effective diffusion coefficient for both models remains the same, however the difference is most prominent in the fast cleaving reactions, or when $\alpha >> 1$. Differences between continuum and discrete stochastic model results have been reported in other studies. For example, in [33] sources of discrepancies in mean first passage times of continuous and discrete models are discussed in detail.

V. DISCUSSION

In this paper we have presented models that describe the removal of a one dimensional track by a cleaving enzyme that interacts with the track components via the hydrolysis of ATP. Our main question, based on the *C. crescentus* chromosomal segregation apparatus, is how bias can be generated in the movement of a cleaving enzyme and subsequently how fast the track edge moves due to the cleaving enzyme action. To answer this question two models, one discrete space and one continuous space, were developed and analyzed. These two models are related to one another in the limit that the size of the cleaving site for the continuous model approaches zero. Using mean first passage time methods for both models, we are able to analytically compute dynamic properties such as track cleaving velocities, and higher moments of cleaving enzyme movement.

We highlight a few results from our models. A key parameter for track cleaving velocities in our models is the non-dimensional variable $\alpha = \frac{g\Delta x^2}{D}$, which specifies the ratio between track cleaving and diffusion rates. When the rate of cleaving reactions exceeds the rate for diffusive transitions between ParA sites ($\alpha >> 1$), the system shows that cleaving velocities cannot exceed simple diffusion driven movement between consecutive cleaving sites. This somewhat counterintuitive result indicates that once cleaving reactions are faster than some basal level, the energy of ATP hydrolysis released during a cleaving reaction does not significantly contribute to track cleaving velocities. Second, using a renewal-reward model, we calculated an effective diffusion coefficient for the CA, which is a measure of effective diffusion of ParB on a ParA track. We find that this diffusion is sensitive to the cleaving rate. For low and high cleaving rates, the effective diffusion limits to the free diffusion coefficient of the CA on the track, indicating that for very slow reactions or very fast reactions the CA is effectively diffusing as a free particle on the track.

For intermediate values of the cleaving rate, however, we find that the effective diffusion coefficient is smaller. This indicates that the ATP hydrolysis energy for these intermediate cleaving rates partially goes toward reducing ParB movements away from the track edge, corresponding to lower diffusion coefficients. Our computations of the higher moments of the CA are in qualitative agreement with dispersions previously calculated in [7, 13]; however in these previous works dispersion is only computed for forward BBM models and we are not aware of results in the forward-backward BBM, which more closely corresponds to our models. The reduced effective diffusion coefficient we found for intermediate cleaving rates is supported by the observed slower diffusion of ParB structures when they come in contact with artificial ParA carpets in [26]; these experimental data might indicate that the cleaving rates for ParB lie in the intermediate range in vivo.

A key assumption that facilitated the development of our model was to view the ParB/ParA complex as a dynamic track altering motor that uses hydrolysis of ParA track components to bias Brownian motion. An important aspect of this modeling is that it allows us to investigate the connection between hydrolysis rates and ParB track-cleaving velocities. In contrast to previous modeling [22, 23] for ParB/ParA interactions, in the models discussed here the ATP hydrolysis rate of a ParB cluster that diffuses on a ParA track is the only source of bias for ParB movement and ParA track cleaving. We find that the rate of hydrolysis of ATP is a key factor when predicting the velocities of the movement of the cleaved edge of a linear filament inside these cells. Specifically, we found that if the ParB cluster has a high hydrolysis efficiency then the cleaving velocity approaches a constant value, corresponding to the diffusive rate of the complex between consecutive sites. These results are in agreement with the simulations of [23]. Our computed effective diffusion also shows that the position of ParB clusters can show a high degree of variability corresponding to free diffusion if the hydrolysis rate is severely weakened; this finding is supported by observations of stalled segregation in ATP hydrolysis mutants [16]. An important contribution of this work is that our simplified modeling framework allows for the calculation of explicit relationships between ParB velocities, ParB diffusion and hydrolysis rates, which has not been previously investigated.

Burnt-bridge models are useful beyond the context of *C. crescentus* segregation. The model proposed in this work can be categorized as a generalization of depolymerization models for bio-polymers. In the cases where the cleaving enzyme is an efficient ATP-ase it will work by removing track components from the ends of the polymer. On the other hand, when ATP hydrolysis rates are lowered, the track experiences shortening by the removal of multiple monomers at a time and the cleaving enzyme positions can experience significant deviation from the track edge. For microtubules, depolymerization is caused by changes in the polymer lattice through GTP-GDP transitions of microtubule tubulin monomers at the polymer ends. However, many proteins that are reported to alter biopolymer depolymerization rates are also found to localize at microtubule ends-the specific role of these proteins in depolymerization velocities is often difficult to discern. For example, the kinesin-13 MCAK [34] interacts with microtubule tip regions and significantly increases depolymerization speed, and katanin proteins ("cellular samurai")[35] literally sever Mts in order to regulate their lengths. The biased diffusion mechanism studied here can have applications in understanding depolymerization models in a more cohesive framework, which allows for the inclusion of the action of "track-cutting" enzymes in depolymerization speeds.

An important question remains open for *C. crescentus* cells, and it has to do with the nature of the ParA structures. Two hypothesis are proposed for ParA organization: an actin-filament based structure [16], where ParA are organized as continuous independent actin filaments inside cells, or a diffusion ratchet setup[20] where ParA forms contiguous dynamic patches on the surface of the nucleoid. In all our models we have assumed that the ParAs form a single continuous track, however, based on these two hypothesis it is possible that ParA arranges into multi-track bundles on the bacterial nucleoid [16]. In an another paper [25], we extend one of our models to a scenario where ParB moves along two parallel filament or tracks. We conclude by noting that the key characteristics of a burnt-bridge model are a continuous structure of ParA proteins, and random site hydrolysis reactions coupled with ParA clearing in the anti-poleward direction. Independent of the details of ParA track structure, our model shows that directed ParB movement can occur when hydrolysis induced cleaving is allowed along the ParA track. Indeed, we propose that the control of this hydrolysis rate might be an important control parameter for these systems.

ACKNOWLEDGEMENTS

This research was supported by National Science Foundation grant DMS 1358932 (BS) and in part by DMS 1122297 (JPK).

VI. APPENDIX

A. Moment calculations for the discrete model

To calculate the moments, we first solve

$$Wx = e_0. \tag{VI.1}$$

The solution has

$$x_j = b\lambda^j, \tag{VI.2}$$

and $x_1 - x_0 = 1$, so that

$$a(\lambda - 1) = 1, \tag{VI.3}$$

which gives that

$$x_j = \frac{\lambda^j}{\lambda - 1},\ j \geq 0, \qquad q_j^\infty = -\alpha x_j,\ j \geq 1. \tag{VI.4}$$

Second, solve

$$Wy = x. \tag{VI.5}$$

For this, we try

$$y_j = a\lambda^j + bj\lambda^j, \tag{VI.6}$$

and find

$$b = \frac{\lambda}{(1-\lambda)(1-\lambda^2)}, \tag{VI.7}$$

and $y_1 - y_0 = x_0 = \frac{1}{\lambda - 1}$ implies

$$a = \frac{1}{(1-\lambda)^2(1-\lambda^2)}. \tag{VI.8}$$

Thus,

$$y_j = \frac{1}{(1-\lambda)(1-\lambda^2)}\Big(\frac{\lambda^j}{1-\lambda} + j\lambda^{j+1}\Big). \tag{VI.9}$$

Now we can calculate all the means. First, an easy check verifies that

$$\mathbf{1}^T q^\infty = -\alpha \sum_{j \geq 1} x_j = 1, \tag{VI.10}$$

as it should. Then,

$$\langle t \rangle = \frac{1}{g\lambda}, \qquad \langle x \rangle = \frac{\Delta x}{1-\lambda}, \qquad v = \frac{g\Delta x\lambda}{1-\lambda}, \tag{VI.11}$$

and the second moments are

$$\langle t^2 \rangle = \frac{2}{g^2\lambda^2}\frac{1+\lambda^2}{1+\lambda}, \qquad \langle x^2 \rangle = \Delta x^2 \frac{1+\lambda}{(1-\lambda)^2}, \qquad \langle xt \rangle = \frac{\Delta x}{g}\frac{\lambda^2+\lambda+1}{\lambda(1-\lambda^2)}. \tag{VI.12}$$

B. Calculations for the continuous model

The steady-state equations for each space interval are

$$0 = Dp_0''(x) + \gamma\phi(x)\sum_{j=1}^{\infty} p_j(x + x_j, t), \qquad 0 < x < L, \tag{VI.13}$$

$$0 = Dp_j''(x), \quad x_{j-1} + L < x < x_j, \quad j = 1, 2, \ldots \tag{VI.14}$$

$$0 = Dp_j''(x) - \gamma\phi(x)p_j(x), \quad x_j < x < x_j + L, \quad j = 1, 2, \ldots. \tag{VI.15}$$

We normalize the area under the curve of the rate function $\phi(x)$ such that $\int_0^L \phi(x)dx = 1$. Since we pick $\phi(x)$ to be proportional to $\chi(x)$, it follows that $\phi(x) = \frac{\chi(x)}{L}$. Rescaling space, $x = \Delta x y$, the problem can be written as

$$0 = p_0''(y) + \frac{\alpha}{k}\sum_{j=1}^{\infty} p_j(y+j,t), \qquad 0 < y < k, \tag{VI.16}$$

$$0 = p_j''(y), \quad j-1+k < y < j, \quad j = 1,2,\ldots \tag{VI.17}$$

$$0 = p_j''(y) - \frac{\alpha}{k}p_j(y), \quad j < y < j+k, \quad j = 1,2,\ldots. \tag{VI.18}$$

where $\alpha = \dfrac{\gamma\Delta x}{D}$, $k = \dfrac{L}{\Delta x}$. Direct integration of eq.(VI.17)-(VI.18) gives,

$$p_j(y) = \begin{cases} a_j + b_j(y-j) & j-1+k < y < j, \\ c_j e^{\hat{\alpha}[y-j]} + d_j e^{-\hat{\alpha}[y-j-k]} & j < y < j+k, \end{cases} \tag{VI.19}$$

for $\hat{\alpha} = \sqrt{\alpha/k}$ and $j = 1,2,\ldots$. Recursive relations for all the coefficients are established by applying appropriate continuity and differentiability conditions at $y = j, j+k$

$$\begin{pmatrix} a_j \\ b_j \end{pmatrix} = \begin{pmatrix} 1 & e^{\hat{\alpha}k} \\ \hat{\alpha} & -\hat{\alpha}e^{\hat{\alpha}k} \end{pmatrix} \begin{pmatrix} c_j \\ d_j \end{pmatrix}, \tag{VI.20}$$

$$\begin{pmatrix} 1 & k-1 \\ 0 & 1 \end{pmatrix} \begin{pmatrix} a_{j+1} \\ b_{j+1} \end{pmatrix} = \begin{pmatrix} e^{\hat{\alpha}k} & 1 \\ \hat{\alpha}e^{\hat{\alpha}k} & -\hat{\alpha} \end{pmatrix} \begin{pmatrix} c_j \\ d_j \end{pmatrix}. \tag{VI.21}$$

The above linear equations can be reduced to a system for only a, b coefficients

$$\begin{pmatrix} a_{j+1} \\ \\ b_{j+1} \end{pmatrix} = \mathbf{A} \begin{pmatrix} a_j \\ \\ b_j \end{pmatrix}, \tag{VI.22}$$

and

$$\mathbf{A} = \begin{pmatrix} \cosh(\hat{\alpha}k) + k_1\sinh(\hat{\alpha}k) & \dfrac{\sinh(\hat{\alpha}k)}{\hat{\alpha}} + k_1\dfrac{\cosh(\hat{\alpha}k)}{\hat{\alpha}} \\ \\ \hat{\alpha}\sinh(\hat{\alpha}k) & \cosh(\hat{\alpha}k) \end{pmatrix}, \tag{VI.23}$$

where $k_1 = (1-k)\hat{\alpha}$. The eigenvalues of A are roots of the characteristic polynomial

$$\lambda^2 - [2\cosh(\hat{\alpha}k) + k_1\sinh(\hat{\alpha}k)]\lambda + 1 = 0, \tag{VI.24}$$

and eigenvectors are

$$V = \begin{pmatrix} \dfrac{\lambda - \cosh(\hat{\alpha}k)}{\hat{\alpha}\sinh(\hat{\alpha}k)} \\ \\ 1 \end{pmatrix}. \tag{VI.25}$$

We construct solutions using the root $\lambda < 1$ of eq. (VI.24) and the corresponding eigenvector V. The resulting solutions are

$$\begin{pmatrix} a_j \\ b_j \end{pmatrix} = C_2\lambda^j V, \tag{VI.26}$$

where the coefficient C_2 is scalar parametrized by α, k.

For the source terms, appearing in $0 < y < k$ interval, we compute

$$h(y) = \chi_{[0<y<k]}(y)\sum_{j=1}^{\infty} p(y+j) \tag{VI.27}$$

$$= C_2\frac{\lambda}{(1-\lambda)(\hat{\alpha}\sinh(\hat{\alpha}k))}[\lambda\cosh(\hat{\alpha}y) - \cosh(\hat{\alpha}(y-k))]. \tag{VI.28}$$

The equation for the first interval $0 < y < k$ is

$$0 = p_0''(y) + \frac{\alpha}{k} h(y), \tag{VI.29}$$

with $p_0'(0) = 0$ and $p_0(k) = a_1 + b_1(k-1)$. The coefficient C_2 is then obtained by applying the normalization condition

$$1 = \int_0^\infty p(y)dy \tag{VI.30}$$

which gives

$$C_2 = \frac{1}{\left(\int_0^k \hat{p}_0(y)dy + \left(\frac{\lambda(1-k)}{(1-\lambda)}\left(\frac{\cosh(\hat{\alpha}k)-\lambda}{\hat{\alpha}\sinh(\hat{\alpha}k)} - \frac{(1-k)}{2}\right)\right) - \frac{\lambda}{\hat{\alpha}^2}\right)} \tag{VI.31}$$

where $\hat{p}_0(y) = p_0/C_2$. Finally, the (dimensional) velocity of track cleaving is calculated using

$$v = \frac{\gamma}{L}\sum_{j=1}^{\infty}\int_0^\infty x_j \chi(x - x_j)p(x)dx. \tag{VI.32}$$

We rescale the velocity $v = \frac{D}{\Delta x}\hat{v}$ where $\hat{v}$ is non-dimensional velocity. This allows us to write

$$\hat{v} = \frac{\gamma \Delta x}{2D}\sum_{j=1}^{\infty}\int_j^{j+k} jp(y)dy \tag{VI.33}$$

$$= C_2 \frac{\lambda}{\lambda - 1}. \tag{VI.34}$$

Two limiting cases for the velocity $k \to 0$ and $k \to 1$ can now be calculated explicitly to obtain

$$\hat{v} = \alpha\frac{2\lambda}{1-\lambda^2}, \quad k \to 0 \quad (L \to 0), \tag{VI.35}$$

$$\hat{v} = \frac{2\hat{\alpha}}{2+\hat{\alpha}}, \quad k \to 1 \quad (L \to \triangle x). \tag{VI.36}$$

These limit calculations agree with our velocity calculations for the limit cases of the continuous model as shown in the manuscript.

C. Moment calculation

The one step-process model reads

$$P_k(i,t) = g\int_{-\infty}^{t}\sum_{j=-\infty}^{i-1} P_{k-1}(j,s)p(n-j, t-s)ds. \tag{VI.37}$$

We calculate various moments for this process by applying the recursive map to the moment expressions.

$$mx_k^1 = \sum_{i=-\infty}^{\infty} iP_k(i,s) \tag{VI.38}$$

$$= g\sum_{i=-\infty}^{\infty} i\int_{-\infty}^{t}\sum_{j=-\infty}^{n-1} P_{k-1}(j,s)p(i-j,t-s)ds \tag{VI.39}$$

$$= g\sum_{i=-\infty}^{\infty}(r+j)\int_{-\infty}^{t}\sum_{r=1}^{\infty} P_{k-1}(i-r,s)p(r,t-s)ds, \quad r = i-j \tag{VI.40}$$

$$= g\sum_{r=1}^{\infty}\int_{-\infty}^{t}(\sum_{i=-\infty}^{\infty}(i-r)P_{k-1}(i-r,s) + r\sum_{i=-\infty}^{\infty} P_{k-1}(i-r,s))p(r,t-s)ds \tag{VI.41}$$

$$= g\sum_{r=1}^{\infty}\int_{-\infty}^{t}(mx_{k-1}^1(s) + r\, mx_{k-1}^0(s))p(r,t-s)ds. \tag{VI.42}$$

We define

$$Mx_k^1 = \int_{-\infty}^{\infty} \sum_{i=-\infty}^{\infty} iP_k(i,t)dt \quad Mt_k^1 = \int_{-\infty}^{\infty} \sum_{i=-\infty}^{\infty} tP_k(i,t)dt, \tag{VI.43}$$

which gives the following relation

$$Mx_k^1 = Mx_{k-1}^1 + Mx_{k-1}^0\langle x\rangle, \quad \langle x\rangle = \sum_{r=1} \int_0^{\infty} r\frac{dq}{dt}dt. \tag{VI.44}$$

Similarly,

$$mt_k^1 = \sum_{n=-\infty}^{\infty} tP_k(n,s) \tag{VI.45}$$

$$= g\sum_{i=-\infty}^{\infty} i\int_{-\infty}^{t} \sum_{j=-\infty}^{i-1} P_{k-1}(j,s)p(i-j,t-s)ds \tag{VI.46}$$

$$= g\sum_{i=-\infty}^{\infty} \int_0^{\infty} t\sum_{r=1}^{\infty} P_{k-1}(i-r,t-u)p(r,u)du, \quad r=i-j, u=t-s \tag{VI.47}$$

$$= g\sum_{r=1}^{\infty} \int_0^{\infty} (\sum_{i=-\infty}^{\infty} (t-u)P_{k-1}(i-r,t-u) + u\sum_{i=-\infty}^{\infty} P_{k-1}(i-r,t-u))p(r,u)du \tag{VI.48}$$

$$= g\sum_{r=1}^{\infty} \int_0^{\infty} (mt_{k-1}^1(t-u) + umt_{k-1}^0(t-u))p(r,u)du. \tag{VI.49}$$

Thus,

$$Mt_k^1 = Mt_{k-1}^1 + Mt_{k-1}^0\langle t\rangle, \quad \langle t\rangle = \sum_{r=1}^{\infty} \int_0^{\infty} up(r,u)du. \tag{VI.50}$$

Further, we note that $Mx_{k-1}^0 = Mt_{k-1}^0 = 1$.

The second moment follows from

$$mx_k^2 = \sum_{i=-\infty}^{\infty} i^2P_k(i,s) \tag{VI.51}$$

$$= g\sum_{i=-\infty}^{\infty} i^2\int_{-\infty}^{t} \sum_{j=-\infty}^{i-1} P_{k-1}(j,s)p(i-j,t-s)ds \tag{VI.52}$$

$$\tag{VI.53}$$

thus

$$Mx_k^2 = Mx_{k-1}^2 + 2Mx_{k-1}^1\langle x\rangle + \langle x^2\rangle, \quad \langle x^2\rangle = \sum_{r=1}^{\infty} \int_0^{\infty} r^2\frac{dq}{dt}dt. \tag{VI.54}$$

In a similar way one calculates equations for the mixed second order moments. For the cross-moments

$$Mxt_k = Mxt_{k-1} + \langle x\rangle Mt_{k-1}^1 + \langle t\rangle Mx_{k-1}^1 + \langle xt\rangle \tag{VI.55}$$

To calculate the variance

$$\sigma x_k^2 \equiv Mx_k^2 - (Mx_k^1)^2 \tag{VI.56}$$

$$= \sigma_{k-1}^2 + \langle x^2\rangle - (\langle x\rangle)^2 \tag{VI.57}$$

$$\tag{VI.58}$$

For the cross-variance we follow a similar approach

$$\rho_k \equiv Mxt_k - Mx_k^1Mt_k^1 \tag{VI.59}$$

$$= \rho_{k-1}^2 + \langle xt\rangle - \langle x\rangle\langle t\rangle. \tag{VI.60}$$

D. Moment calculations for delta function rates

For the continuous problem formulation,

$$\frac{\partial p}{\partial t} = D\frac{\partial^2 p}{\partial x^2} - \gamma \sum_i \delta(x - x_i)p + \gamma\delta(x)\sum_i p(x + x_i). \tag{VI.61}$$

the first exit formulation, using the p, q probabilities, is

$$\frac{\partial p}{\partial t} = D\frac{\partial^2 p}{\partial x^2} - \gamma \sum_i \delta(x - x_i)p, \tag{VI.62}$$

$$\frac{dq_i}{dt} = \gamma p(x_i). \tag{VI.63}$$

In operator notation the problem can we written as

$$\frac{\partial p}{\partial t} = Wp, \tag{VI.64}$$

$$\frac{\partial q_i}{\partial t} = \gamma p(x_i), \tag{VI.65}$$

where

$$W = D\frac{\partial^2}{\partial x^2} - \gamma \sum_i \delta(x - x_i). \tag{VI.66}$$

Then, using the same approach as in the discrete model section we obtain the relevant probabilities and exit times

$$q_i^\infty = -\gamma e_0^T W^{-T}\delta(x - x_i), \qquad Tq_i^\infty = \gamma e_0^T W^{-2T}\delta(x - x_i), \qquad T^2 q_i^\infty = -\gamma 2 e_0^T W^{-3T}\delta(x - x_i). \tag{VI.67}$$

Since the PDE operator W is self-adjoint $W = W^T$, the object $\pi_i = -\gamma W^{-T}\delta(x - x_i)$ satisfies

$$W\pi_i = -\gamma\delta(x - x_i), \tag{VI.68}$$

and $G_i = \gamma W^{-2T}\delta(x - x_i)$ satisfies

$$WG_i = -\pi_i. \tag{VI.69}$$

Further, $T_i^2 = -\gamma 2W^{-3T}\delta(x - x_i)$ satisfies

$$WT_i^2 = -2G_i. \tag{VI.70}$$

Therefore, we have three equations that are relevant for moment calculations for the continuous problem

$$D\frac{d^2\pi_i}{dx^2} - \gamma \sum_{j>0} \delta(x - x_j)\pi_i = -\gamma\delta(x - x_i), \tag{VI.71}$$

$$D\frac{d^2 G_i}{dx^2} - \gamma \sum_{j>0} \delta(x - x_j)G_i = -\pi_i(x), \tag{VI.72}$$

$$D\frac{d^2 T_i^2}{dx^2} - \gamma \sum_{j>0} \delta(x - x_j)T_i^2 = -2G_i(x), \tag{VI.73}$$

The moments we want can be computed using

$$\langle t\rangle = \sum_i G_i(0), \qquad \langle t^2\rangle = \sum_i T_i^2(0), \tag{VI.74}$$

and

$$\langle x\rangle = \Delta x \sum_i i\pi_i(0), \qquad \langle x^2\rangle = \Delta x^2 \sum_i i^2\pi_i(0), \qquad \langle xt\rangle = \Delta x \sum_i iG_i(0). \tag{VI.75}$$

To find $\pi_i(x)$, set

$$\pi_i(x) = \pi_j^i + s_j^i(x - x_j), \tag{VI.76}$$

$$s_j^i \Delta x = \pi_{j+1}^i - \pi_j^i, \tag{VI.77}$$

for $x_j < x < x_{j+1}$. Then, the governing equation (VI.71) reduces to the linear system

$$\pi_{j-1}^i - (2+\alpha)\pi_j^i + \pi_{j+1}^i = -\alpha\delta_{ij}, \tag{VI.78}$$

where $\alpha = \frac{g\Delta x^2}{D}$, and $\pi_0^i = \pi_1^i$. Try a solution

$$\pi_j^i = \begin{cases} c_1^i(\lambda^j + \lambda^{1-j}) & j \le i \\ c_2^i \lambda^{j-i-1} & j > i \end{cases}. \tag{VI.79}$$

We find

$$c_1^i = \frac{\alpha\lambda^i}{1-\lambda^2}, \qquad c_2^i = \frac{\alpha}{1-\lambda^2}(\lambda^{2i+1} + \lambda^2), \tag{VI.80}$$

so that

$$\pi_j^i = \frac{\alpha}{1-\lambda^2}(\lambda^{i+j} + \lambda^{1+|i-j|}), \tag{VI.81}$$

$$\pi_0^i = \frac{\alpha\lambda^i}{1-\lambda}, \qquad i > 0, \tag{VI.82}$$

which is the same as the discrete space problem. Then, some moments are

$$\langle x\rangle = \Delta x \sum_i i\pi_0^i = \frac{\Delta x}{1-\lambda}, \qquad \langle x^2\rangle = \Delta x^2 \frac{\lambda+1}{(1-\lambda)^2}, \tag{VI.83}$$

which are exactly the same as for the discrete space problem.

To find $\langle t\rangle$, we note that $\langle t\rangle = G(0)$, where $G = \sum_i G_i$ satisfies

$$D\frac{d^2G}{dx^2} - \gamma \sum_{j>0} \delta(x - x_j)G = -1, \tag{VI.84}$$

since $\sum_i \pi_i(x) = 1$. So,

$$G(x) = g_i + h_i(x - x_i) - \frac{(x-x_i)^2}{2D}, \qquad x_i < x < x_{i+1}. \tag{VI.85}$$

It follows that

$$g_{i+1} = g_i + h_i\Delta x - \frac{\Delta x^2}{2D}, \tag{VI.86}$$

and

$$h_i - h_{i-1} + \frac{\Delta x}{D} - \frac{\gamma}{D}g_i = 0, \tag{VI.87}$$

with the initial condition $h_0 = 0$, which simplifies to

$$g_{i+1} - 2g_i + g_{i-1} - \alpha g_i = -\frac{\Delta x^2}{D}. \tag{VI.88}$$

It follows that

$$g_i = \frac{1}{g}\Big(1 + \frac{\alpha}{2}\frac{\lambda^i}{1-\lambda}\Big), \tag{VI.89}$$

so that

$$\langle t\rangle = g_0 = \frac{1+\lambda}{2g\lambda}. \tag{VI.90}$$

Notice that

$$v = \frac{\langle x\rangle}{\langle t\rangle} = \frac{2\gamma\lambda}{1-\lambda^2}, \tag{VI.91}$$

which agrees with the equation (III.12).

Now to determine $\langle t^2\rangle = T^2(0)$ where $T^2(x) = \sum_i T_i^2(x)$ satisfies

$$D\frac{d^2T^2}{dx^2} - \gamma\sum_{j>0}\delta(x-x_j)T^2 = -2G(x). \tag{VI.92}$$

We solve this equation in the same way as above and obtain

$$\langle t^2\rangle = \frac{1}{12g^2}\frac{\lambda^4+8\lambda^3+22\lambda^2+12\lambda+5}{\lambda^2(\lambda+1)}. \tag{VI.93}$$

To calculate $\langle xt\rangle = X(0)$, we must solve the differential equation for $X(x) = \Delta x\sum_i iG_i(x)$,

$$D\frac{d^2X}{dx^2} - \gamma\sum_{j>0}\delta(x-x_j)X = -\Delta x\sum_i i\pi_i(x). \tag{VI.94}$$

which gives

$$\langle xt\rangle = \frac{\Delta x}{6g}\frac{\lambda^3+7\lambda^2+7\lambda+3}{\lambda(1-\lambda^2)}. \tag{VI.95}$$

Now we can calculate the variance of the renewal-reward process to be

$$\nu^2 = \langle x^2\rangle - 2v\langle xt\rangle + v^2\langle t^2\rangle \tag{VI.96}$$

$$= \frac{2\Delta x^2}{3}\Big(\frac{\lambda^4+2\lambda^3+6\lambda^2+2\lambda+1}{(1-\lambda)^2(1+\lambda)^3}\Big), \tag{VI.97}$$

and consequently the relative effective diffusion is

$$\frac{\nu^2}{\mu_1}\frac{1}{D} = \frac{4}{3}\frac{\lambda^4+2\lambda^3+6\lambda^2+2\lambda+1}{(1+\lambda)^4}. \tag{VI.98}$$

[1] J. Howard, Nature **389**, 561 (1997).
[2] F. Jülicher, A. Ajdari, and J. Prost, Reviews of Modern Physics **69**, 1269 (1997).
[3] A. Gennerich and R. D. Vale, Current Opinion in Cell Biology **21**, 59 (2009).
[4] S. Saffarian, I. E. Collier, B. L. Marmer, E. L. Elson, and G. Goldberg, Science **306**, 108 (2004).
[5] S. Saffarian, H. Qian, I. Collier, E. Elson, and G. Goldberg, Phys. Rev. E **73**, 041909 (2006).
[6] T. Antal and P. Krapivsky, Physical Review E **72**, 046104 (2005).
[7] A. Y. Morozov, E. Pronina, A. B. Kolomeisky, and M. N. Artyomov, Physical Review E **75**, 031910 (2007).
[8] A. Y. Morozov and A. B. Kolomeisky, Journal of Statistical Mechanics: Theory and Experiment **2007**, P12008 (2007).
[9] J. Mai, I. M. Sokolov, and A. Blumen, Phys. Rev. E **64**, 011102 (2001).
[10] A. Lakhanpal and T. Chou, Physical review letters **99**, 248302 (2007).
[11] T. Omabegho, R. Sha, and N. C. Seeman, Science **324**, 67 (2009).
[12] J. H. Schulz, A. B. Kolomeisky, and E. Frey, EPL (Europhysics Letters) **95**, 30004 (2011).

[13] M. N. Artyomov, A. Y. Morozov, E. Pronina, and A. B. Kolomeisky, Journal of Statistical Mechanics: Theory and Experiment **2007**, P08002 (2007).
[14] M. N. Artyomov, A. Y. Morozov, and A. B. Kolomeisky, Physical Review E **77**, 040901 (2008).
[15] T. Antal, P. L. Krapivsky, and S. Redner, Phys. Rev. E **72**, 036121 (2005).
[16] J. L. Ptacin, S. F. Lee, E. C. Garner, E. Toro, M. Eckart, L. R. Comolli, W. Moerner, and L. Shapiro, Nature cell biology **12**, 791 (2010).
[17] W. B. Schofield, H. C. Lim, and C. Jacobs-Wagner, The EMBO journal **29**, 3068 (2010).
[18] S. Ringgaard, J. van Zon, M. Howard, and K. Gerdes, Proceedings of the National Academy of Sciences **106**, 19369 (2009).
[19] K. Gerdes, M. Howard, and F. Szardenings, Cell **141**, 927 (2010).
[20] A. G. Vecchiarelli, L. C. Hwang, and K. Mizuuchi, Proceedings of the National Academy of Sciences **110**, E1390 (2013).
[21] A. G. Vecchiarelli, Y.-W. Han, X. Tan, M. Mizuuchi, R. Ghirlando, C. Biertümpfel, B. E. Funnell, and K. Mizuuchi, Molecular microbiology **78**, 78 (2010).
[22] B. Shtylla and J. P. Keener, Journal of Theoretical Biology **307**, 82 (2012).
[23] E. Banigan, M. Gelbart, Z. Gitai, A. Liu, and N. Wingreen, Bulletin of the American Physical Society **56** (2011).
[24] B. Derrida, Journal of Statistical Physics **31**, 433 (1983).
[25] B. Shtylla and J. P. Keener, submitted (2014).
[26] A. G. Vecchiarelli, K. C. Neuman, and K. Mizuuchi, Proc Natl Acad Sci U S A (2014), 10.1073/pnas.1401025111.
[27] G. Laloux and C. Jacobs-Wagner, J Cell Biol **201**, 827 (2013).
[28] N. G. Van Kampen, *Stochastic processes in physics and chemistry*, Vol. 1 (Access Online via Elsevier, 1992).
[29] D. T. Gillespie, The journal of physical chemistry **81**, 2340 (1977).
[30] H. C. Tijms, *A first course in stochastic models* (Wiley. com, 2003).
[31] R. Wolff, *Stochastic Modeling and the Theory of Queues* (Prentice Hall, 1989).
[32] C. W. Gardiner, *Handbook of Stochastic Methods for Physics, Chemistry and the Natural Sciences (Third Edition)* (Springer, 2004).
[33] C. R. Doering, K. V. Sargsyan, L. M. Sander, and E. Vanden-Eijnden, Journal of Physics: Condensed Matter **19**, 065145 (2007).
[34] J. Helenius, G. Brouhard, Y. Kalaidzidis, S. Diez, and J. Howard, Nature **441**, 115 (2006).
[35] L. Quarmby, Journal of cell science **113**, 2821 (2000).